

VLT+UVES SPECTROSCOPY OF THE CA II LOBAL QUASAR SDSS 0300+0048¹

Patrick B. Hall^{2,3}, Damien Hutsemekers^{4,5}, Scott F. Anderson⁶, J. Brinkmann⁷, Xiaohui Fan^{8,9}, Donald P. Schneider¹⁰, Donald G. York^{11,12}
 Draft version May 21, 2019

ABSTRACT

We study high-resolution spectra of the ‘overlapping-trough’ low-ionization broad absorption line (LoBAL) quasar SDSS 0300+0048. The Ca II, Mg II and Mg I column densities in SDSS 0300+0048 are the largest reported to date for any BAL outflow. The broad Ca II absorption in this object is mildly blended, but the blending can be disentangled to measure the Ca II column density, which is large enough that the outflow must include a strong hydrogen ionization front. The outflow begins at a blueshift of 1650 km s^{-1} from the systemic redshift. The lowest velocity BAL region produces strong Ca II absorption but does not produce significant excited Fe II absorption, while the higher velocity excited Fe II absorption region produces very little Ca II absorption. This segregation can only really be explained by a disk wind outflow. Whether the outflow is smooth or clumpy, we conclude that the Ca II BAL region has a density high enough to populate excited levels of Fe II, but a temperature low enough to prevent them from being significantly populated. This requirement means the Ca II BAL region has $T \sim 1100 \text{ K}$, and perhaps even $T \sim 550 \text{ K}$. This object also has an associated absorption line system (AAL) which exhibits partial covering, and therefore is likely located near the central engine. Whether or not it is associated with the BAL outflow is unclear. Blending of the AAL with the BAL trough shows that the spatial region covered by the BAL outflow can vary over velocity differences of 1700 km s^{-1} .

Subject headings: quasars: absorption lines, quasars: general, quasars: emission lines

1. introduction

One of the goals of the Sloan Digital Sky Survey (SDSS; York et al. 2000) is to obtain spectra for 10^5 quasars to $i = 19.1$ ($i = 20.2$ for $z > 3$ candidates), in addition to the 10^6 galaxies which comprise the bulk of the spectroscopic targets (Blanton et al. 2003). From astrometrically calibrated drift-scanned imaging data (Gunn et al. 1998; Pier et al. 2003) on the SDSS ugriz AB \sin^2 magnitude system (Fukugita et al. 1996; Lupton, Gunn, & Szalay 1999; Hogg et al. 2001; Stoughton et al. 2002; Smith et al. 2002), quasar candidates are selected primarily using color criteria designed to target objects whose broad-band colors are different from those of normal stars and galaxies (Richards et al. 2002). Due to these inclusive criteria, the selection of candidates using i band magnitudes rather than blue magnitudes (which are more affected by absorption and reddening), and its area and depth, the SDSS is effective at finding unusual quasars (e.g., Fan et al. 1999). Many of these objects are unusual broad absorption line (BAL) quasars.

BAL quasars show absorption from gas with typical outflow velocities of $0.1c$ (Weymann et al. 1991) and mass loss rates probably comparable to the accretion rates required to power quasars ($1 M_{\odot} \text{ yr}^{-1}$). Therefore an understanding of BAL outflows is required for an understanding of quasars as a whole. Usually BAL troughs are only seen in high ionization species, but about 15% of BAL quasars also show absorption from low ionization species, including absorption of excited states or terms of Fe II and Fe III in rare cases. In Hall et al. (2002, hereafter H02) we presented several examples of ‘overlapping-trough’ BAL quasars whose flux shortward of Mg II is almost completely absorbed by troughs of excited Fe II. In this paper we present a high-resolution spectrum of one such object, SDSS 0300+0048 at $z = 0.89$, and use it to constrain the column densities and possible structure of its impressive outflow. SDSS 0300+0048 is only the fourth quasar known to have a Ca II BAL trough ($\times 5.2$ of H02),¹³ and only the second to be studied at high

¹ Based on observations from ESO Director’s Discretionary Time program 267A-5698.

² Princeton University Observatory, Princeton, NJ 08544

³ Departamento de Astronomía y Astrofísica, Facultad de Física, Pontificia Universidad Católica de Chile, Casilla 306, Santiago 22, Chile

⁴ Research Associate FNRS, University of Liege, Allée du 6 août 17, Bat. 5c, 4000 Liege, Belgium

⁵ European Southern Observatory, Casilla 19001, Santiago, Chile

⁶ University of Washington, Department of Astronomy, Box 351580, Seattle, WA 98195

⁷ Apache Point Observatory, P.O. Box 59, Sunspot, NM 88349-0059

⁸ Institute for Advanced Study, Olden Lane, Princeton, NJ 08540

⁹ Current affiliation: Steward Observatory, The University of Arizona, Tucson, Arizona 85721

¹⁰ Department of Astronomy and Astrophysics, The Pennsylvania State University, University Park, PA 16802

¹¹ The University of Chicago, Department of Astronomy and Astrophysics, 5640 S. Ellis Ave., Chicago, IL 60637

¹² The University of Chicago, Enrico Fermi Institute, 5640 S. Ellis Ave., Chicago, IL 60637

¹³ Rupke, Veilleux, & Sanders (2002) have found that ultraluminous infrared galaxies can have Ca II outflows with large rest-frame equivalent widths (REW s). It is unclear how similar these narrower outflows are to Ca II BALs. The continuum around Ca II in most of their objects is dominated by galaxy light; the addition of a quasar continuum might greatly decrease the REW s. In any case, the outflows in SDSS 0300+0048 and Q 2359-1241 set in well shortward of the systemic redshifts, which differentiates them from the outflows studied by Rupke et al. (2002).

resolution, after Q 2359 1241 (Arav et al. 2001). Both quasars have "detached" absorption troughs which do not start at the systemic redshift: those in Q 2359 1241 set in 750 km s^{-1} shortward, and those in SDSS 0300+0048 1700 km s^{-1} shortward. SDSS 0300+0048 also has a strong, narrow associated absorption system at the systemic redshift, with $Mg II$ $REW = 1.882 \text{ \AA}$. Whether this system is intrinsic to the nuclear regions of the quasar is one issue we discuss in this paper. We begin with a discussion of the most common method of analyzing intrinsic absorption lines, then we apply this method to SDSS 0300+0048, and finally we discuss our results.

2. analyzing intrinsic absorption lines

Suppose we observed unblended doublet absorption from a BAL region covering a fraction C of the quasar's light with an optical depth τ . The resulting normalized residual intensities in the two lines of the doublet as a function of velocity v are:

$$I_1(v) = 1 - C_v(1 - e^{-\tau_1}) \quad (1)$$

$$I_2(v) = 1 - C_v(1 - e^{-R\tau_1}) \quad (2)$$

where $R = g_2 f_2 \lambda_2 / g_1 f_1 \lambda_1$ is the ratio of the optical depth of line 2 to that of line 1 (the g_i are the statistical weights, the f_i the oscillator strengths, and the λ_i the wavelengths of the lines). Our convention is that I_1 refers to the stronger line of the doublet and τ_1 refers to the optical depth in that line. For any doublet with $R = 0.5$, such as $Mg II$ and $Ca II$, these equations yield the following solutions (Hamann et al. 1997) and associated uncertainties for C_v and τ_1 :

$$C_v = \frac{1 + \frac{I_2^2}{I_1^2} - \frac{2I_2}{I_1}}{1 + \frac{I_2^2}{I_1^2} - \frac{2I_2}{I_1}}; \quad \tau_1 = \frac{\ln \left(\frac{1 + \frac{I_2^2}{I_1^2} - \frac{2I_2}{I_1}}{1 + \frac{I_2^2}{I_1^2} - \frac{2I_2}{I_1}} \right)}{\ln \left(\frac{1 + \frac{I_2^2}{I_1^2} - \frac{2I_2}{I_1}}{1 + \frac{I_2^2}{I_1^2} - \frac{2I_2}{I_1}} \right)} \quad (3)$$

$$\tau_1 = \ln \frac{I_1(1 + C_v)}{C_v} = 2 \ln \frac{I_2 - \frac{I_1}{R}}{1 - \frac{I_1}{R}}; \quad \tau_2 = \frac{2e^{-\tau_1}(I_2 - \frac{I_1}{R})}{(I_2 - \frac{I_1}{R})^2} \frac{1}{\frac{2}{I_1} + \frac{2}{I_2} \frac{I_1}{I_2} - 1} \quad (4)$$

where it is understood that I_1 and I_2 are functions of velocity. The solution for C_v , and thus for τ_1 as well, is only physical ($0 \leq C_v \leq 1$) when

$$0 \leq I_1 \leq 1 \text{ and } 0 \leq I_2 \leq 1 \text{ and } \frac{I_2^2}{I_1^2} \leq I_1 \text{ and } I_2 \leq I_1 \quad (5)$$

The last of the above conditions could be violated in the case of saturated absorption partially filled in by optically thin emission from the same doublet transition responsible for the absorption. The next to last could be invalidated by the presence in the spectrum of significant host galaxy or scattered quasar light.

The above equations can also break down if there are different covering factors for different emission regions (e.g., the continuum source, the broad emission line (BEL) region, and the Fe II emission region; see x4.3.2 and Ganguly et al. 1999) or if the emissivities of the covered and uncovered regions are different functions of velocity (as pointed out by Srianand & Shankaranarayanan 1999 and observed by, e.g., Gabel 2002). Moreover, the assumption that a fraction C of the quasar's light is occulted at a single optical depth τ and that the remaining light is unobscured is likely to itself be an approximation (de Kool, Korista, & Arav 2002b), and would be inappropriate if there are cases where the resonance scattering interpretation of BAL quasars is correct (Branch et al. 2002). Nevertheless, the above equations are useful for studying BAL troughs, even if only to verify that one or more of the above complications is occurring.

If the absorption is broad enough that the two lines of the doublet are blended over a velocity width v_b which is less than their velocity separation v , then there are three distinct velocity regimes to consider, which we label A to C from high velocity to low. In A and C one of the two lines produces blended absorption; in B neither line is blended (see x4.3.1 for a concrete example). Using positive v to denote outflows (absorption at shorter wavelengths) and assuming the stronger line (subscript 1) is the shorter wavelength one yields:

$$\text{A : } v_{\text{max}} > v > v_{\text{max}} - v_b \quad v + v_b : \quad I_1 = 1 - C_v(1 - e^{-\tau_1}) \quad (6)$$

$$I_2 = [1 - C_v(1 - e^{-R\tau_1})] [1 - C_{v+v_b}(1 - e^{-\tau_2})] \quad (7)$$

$$\text{B : } v_{\text{max}} - v_b > v > v_{\text{max}} - v \quad v : \quad I_1 = 1 - C_v(1 - e^{-\tau_1}) \quad (8)$$

$$I_2 = 1 - C_v(1 - e^{-R\tau_1}) \quad (9)$$

$$\text{C : } v_{\text{max}} - v > v > v_{\text{max}} - v - v_b \quad v - v_b : \quad I_1 = [1 - C_v(1 - e^{-\tau_1})] [1 - C_{v-v_b}(1 - e^{-R\tau_2})] \quad (10)$$

$$I_2 = 1 - C_v(1 - e^{-R\tau_1}) \quad (11)$$

where v_{max} is the maximum outflow velocity and C_{v-v_b} and C_{v+v_b} are the covering factors and optical depths at velocities $v - v_b$ and $v + v_b$. If blending does not occur ($v_b = 0$), regimes B and C vanish and regime A reduces to Eqs. 1-2 since C_{v-v_b} and C_{v+v_b} become undefined. Both C and τ will be defined only over a velocity range less than v . Otherwise, the convolution symbols indicate that the observed spectrum is affected by absorption from both lines in a possibly complicated manner. Nonetheless, since the C_{v-v_b} and C_{v+v_b} are just the values of C_v and τ_1 in regime B, which can be solved for, it may be possible to estimate the C_v and τ_1 in regimes A and C. For example, if C_v is a constant and a fixed emission region is covered at all velocities, the convolutions are simple multiplications. This is not the case if C_v varies or if different emission regions are covered as a function of velocity, even if C_v is numerically constant.

3. vlt + uves observations of sdss 0300+ 0048

Observations of several SDSS BAL quasars were obtained on UT 10-12 Aug 2001 using the ESO Very Large Telescope (VLT) Unit 2 (Kueyen) and Ultra-Violet Echelle Spectrograph (UVES). This section provides observational details for all objects; science results for SDSS 2215+0045 and SDSS 1453+0029 can be found in Hall & Hutsemekers (2003). A $1''$ slit was used, yielding a resolution $R \sim 40,000$ (7.5 km s^{-1}) at all wavelengths. A depolarizer was also used for all observations. Each exposure was reduced individually with optimum extraction (Horne 1986), including simultaneous background and sky subtraction. Since the shortest wavelength setting for SDSS 0300+0048 had a very low signal-to-noise ratio and yielded different results for the two exposures, it is not used in this paper. The extraction for the next shortest wavelength was determined manually in places where the flux was zero over several orders. Telluric absorption lines were removed for the red settings using observations of telluric standard stars, shifted in velocity according to the different times of the observations and scaled in intensity according to the airmass difference. Whenever two or three exposures of each setting were available, they were averaged with rejection of cosmic rays and known CCD artifacts. Finally, all settings were rebinned to a constant wavelength interval of 0.015 Å on a vacuum heliocentric scale, scaled in intensity by the overlap regions where needed, and merged into a single spectrum.

4. analyzing sdss 0300+ 0048

Figure 1 shows a portion of the SDSS spectrum of SDSS 0300+0048, intended to help put in context the small regions of high-resolution UVES spectra we will present in this paper. From the associated absorber's central subsystem seen in Ca II 3969 and Mg I in the UVES spectrum, we adopt a systemic redshift of $z = 0.891850 \pm 0.000005$, in excellent agreement with the value $z = 0.89191 \pm 0.00005$ measured from the SDSS spectrum. There is weak [O II] emission at $z = 0.8908 \pm 0.0007$, a blueshift of $166 \pm 111 \text{ km s}^{-1}$ (using 3728.48 Å for the unresolved doublet's vacuum rest wavelength).

4.1. What is the Continuum?

To properly analyze the absorption in SDSS 0300+0048, we must know or be able to model its intrinsic continuum at the relevant wavelengths. To do this for the transitions of interest in SDSS 0300+0048 (Mg II, Mg I and Ca II) requires the matching of complex blends of iron emission and absorption.

Figure 2 shows the SDSS rest frame spectrum of SDSS 0300+0048 (solid line). The emission features longward of Mg II are plausibly identifiable as blends of Fe II and Fe I, as discussed in §5.2 of H02, though we now recognize that Tiii emission is also likely to contribute (Kwan et al. 1995). The dashed line shows one possible model for the unabsorbed continuum of SDSS 0300+0048, consisting of a flat-in-F power-law plus a scaled and smoothed iron emission template. This template was constructed by fitting and subtracting a power-law to the spectrum of a bright, narrow-lined, strong Fe II-emitting quasar from the SDSS using continuum windows at 1680-1700 Å and 3675-3710 Å. Since the template is intended for illustrative purposes only, no attempt was made to exclude emission from Mg II or other non-iron transitions (or to optimize the slope of the power-law continuum component of the model spectrum). This model spectrum is a good match to the emission feature just shortward of 3000 Å, the blue side of which may be affected by absorption, and to the wavelength extent of the weak feature at 3400-3600 Å. However, this latter feature is much stronger than in the model; SDSS 0300+0048 has emission features at 3025 Å and 3250 Å not seen in the model (the latter could be Tiii), and there are two features around 3100 Å in the template which are not seen in SDSS 0300+0048. Given these discrepancies between the model spectrum and the observed spectrum, we cannot use the model spectrum to predict the intrinsic continuum of SDSS 0300+0048 at $< 2900 \text{ Å}$ with any confidence. In the future it may be possible to find another strong Fe II-emitting quasar whose spectrum better matches that of SDSS 0300+0048 at $> 3000 \text{ Å}$, but this is the best match we have found to date in the SDSS or in the literature (e.g., Graham, Clowes, & Campaniano 1996). Note that the Fe emission templates of Boroson & Green (1992) and Vestergaard & Wilkes (2001) only cover 4250-7000 Å and 1250-3090 Å, respectively.

Alternatively, if we could match the $> 3000 \text{ Å}$ spectrum of SDSS 0300+0048 using a theoretical model, we could use that model to predict its unabsorbed continuum at $< 3000 \text{ Å}$. However, published theoretical Fe II emission models either do not extend to $> 3200 \text{ Å}$ (Verner et al. 1999) or do not include sufficient transitions at $> 3200 \text{ Å}$ to match observations (Sigut & Pradhan 2002), and the situation for other possibly important ions such as Fe I and Tiii is no better.

Thus at present we have no reliable model for the unabsorbed continuum of SDSS 0300+0048 at the wavelengths of Mg II, Mg I or Ca II. For Ca II, we can construct a reasonable local continuum. For Mg II, Mg I and other transitions at even shorter wavelengths we must keep in mind that a local continuum estimate probably underestimates the unabsorbed continuum by a factor of 2, unless dust reddening produces a turnover in the unabsorbed spectrum.

4.2. The Associated Absorption

To remove the narrow associated Ca II 3934 blended with the broad Ca II 3969, we must model the associated system. This procedure yielded interesting results, but ones tangential to the main paper, and so is discussed in Appendix A.

4.3. The Broad Absorption

4.3.1. Overview

Figure 3 shows the normalized spectrum of SDSS 0300+0048 around the broad absorption troughs of five separate transitions. The heavier lines denote spectral regions that are not confused with absorption from different transitions. Each transition has unique, unconfused velocity ranges, as we now discuss.

Mg II is confused with Fe II 2773 (UV 63) at $> 7150 \text{ km s}^{-1}$. Since the Mg II absorption starts at about 1650 km s^{-1} , the Mg II trough is at least 5500 km s^{-1} wide. An upper limit to its width is impossible to determine, given that the continuum does not return to its unabsorbed level anywhere shortward of Mg II (Figure 1). However, a reasonable maximum velocity can be inferred from the Fe II UV 63 absorption, which tapers out at 10850 km s^{-1} for the UV 63 multiplet line with the shortest wavelength (2715 Å). That maximum velocity implies a Mg II trough at least 9200 km s^{-1} broad.

The Mg I absorption appears to start when the Mg II trough appears to saturate, at 2000 km s^{-1} . It is unclear just how high a velocity the Mg I absorption reaches, both because Mg I is confused with associated Mg II at $> 5200 \text{ km s}^{-1}$ and because the continuum normalization between Mg I and Mg II is very uncertain. The Mg I might reach only 4000 km s^{-1} , matching the strong Ca II absorption, in which case the alternate continuum normalization shown by the tilted dashed line in the Figure would be more appropriate. Alternatively, the Mg I might reach 6400 km s^{-1} , matching the possible highest-velocity Ca II, or even extend to $> 7150 \text{ km s}^{-1}$ like Mg II in which case it would overlap with Mg II.

The broad Ca II was normalized by a simple linear continuum fit to two narrow wavelength regions around 7294 Å and 7478 Å. To determine the blending in Ca II, we use the fact that Ca II 3934 is the stronger line of the doublet, which means we can be sure that the highest velocity detectable absorption is from it and not from even higher velocity Ca II 3969. The Ca II 3934 absorption does not appear to reach velocities as large as the Mg II absorption does, but instead tapers out at 5657 km s^{-1} . Given that the velocity separation of the Ca II doublet is 2640.1 km s^{-1} , the Ca II 3934 trough is unblended only at $3017\text{--}5657 \text{ km s}^{-1}$. Similarly, since the Ca II 3969 absorption only starts at 1697 km s^{-1} , the Ca II 3969 trough is unblended only at $1697\text{--}4337 \text{ km s}^{-1}$ (discounting the narrow associated Ca II 3934 near 2640 km s^{-1}).

As first noted in H02, the Fe II 2632 absorption (from excited *n*-structure levels in the ground state) does not start at the same velocity as the Mg II absorption. Despite slight contamination from associated Fe II 2600, it is clear that the broad Fe II 2632 absorption begins at a velocity which matches the highest-velocity component of the main Ca II trough (see x5.1). As with Mg II, the high-velocity limit of the Fe II 2632 absorption is likely to be the same as that of the Fe II UV 63 absorption: 10850 km s^{-1} .

4.3.2. Broad Ca II Absorption: Velocity Regime B

To begin the quantitative analysis of the broad Ca II absorption, we used Eqs. 8–9 to solve for C_v and v_v in the unblended outflow at $3017\text{--}4337 \text{ km s}^{-1}$ (velocity regime B). The results are shown in Figure 4, where the original pixels have been binned by a factor of 5 in order to achieve an acceptable signal-to-noise ratio (S/N). We defer a detailed discussion of this Figure until later in this section. Note that no points are plotted for velocity bins where the residual intensities do not allow a physical solution because one or more of the conditions of Equation 5 are violated. This situation occurs for 37% of the original pixels in velocity regime B. Inspection of the velocities where the residual intensities did not allow a physical solution suggested that our continuum normalization was an underestimate. Thus we re-fit using a third-order Legendre polynomial between two narrow wavelength regions around 7278 Å and 7496 Å. This normalization yielded only a slight increase in the number of pixels where the residual intensities allow a physical solution, suggesting that our continuum normalization is not the major source of error in that respect.

One possible source of error is scattered light (or host galaxy light) which does not pass through the BAL region and thus fills in the absorption troughs. Host galaxy light should be a $< 1\%$ effect since this quasar is quite luminous ($M_i = -27.23$). Since the observed minimum residual intensity in the broad Ca II trough is $6.0 \pm 1.5\%$ of the continuum, that is the maximum percentage that unabsorbed scattered light can contribute to the observed continuum. To test the effects of a maximal contribution from unabsorbed scattered light, we subtracted 0.06 from the residual intensity at all velocities, renormalized by 0.94, and repeated our calculation of C and v . This adjustment slightly decreased the number of pixels with allowed physical solutions, suggesting that ignoring the contribution of scattered light does not greatly affect the calculation of C_v and v_v .

Another possible source of error is our assumption that the covering factor is the same for the featureless continuum source and Fe II emission regions. Doublet absorption does not provide enough information to solve for two covering factors independently. However, x4.2 of Ganguly et al. (1999) discusses how joint constraints on C_c and C_{Fe} can still be made, given the ratio W of the Fe II flux to the continuum source flux. For a lower limit of $W = 0.07$ in SDSS 0300+0048, the situation lies in between that of a single covering factor and the scattered light case considered previously, so assuming a single covering factor is reasonable. In the more realistic $W = 0.27$ case, the covering factors have similar, large values (maximum of $C_c > 0.92$ and $C_{Fe} > 0.72$) and assuming a single covering factor again appears reasonable.¹⁴

Neither the details of the assumed continuum, the neglect of scattered light, or the assumption of a single covering factor appear responsible for the relatively large fraction of pixels (37%) for which the residual intensities in the Ca II doublet lines do not allow a physical solution for C_v and v_v . The explanation for these pixels must lie primarily in the random noise. This explanation is consistent with Figure 4, which shows that the bulk of the pixels without physical solutions lie in the regions of weak absorption, where the noise is comparable to the strength of the absorption. (The average S/N per pixel in the Ca II trough is 17, with a range between 8 and 24.)

Considering Figure 4 in more detail, we see that in many individual velocity bins (each consisting of five original pixels) both the minimum C_v solution (thin red line) and the $C_v = 1$ solution are formally acceptable at the 68% confidence level (1σ). However, the lower panel of Figure 4 shows that overall the covering factor in the unblended outflow is

¹⁴ We cannot rule out an Fe II emission region which remains uncovered until the continuum emission region is fully covered, and thus has $C_{Fe} = 0$ at most velocities, but fitting C_v and v_v for such a scenario yields a large increase in the number of pixels which do not correspond to a physical solution.

statistically inconsistent with both limiting cases. Neither $C_v = 1$ at all velocities nor C_v having its minimum value at all velocities are good fits to the data as a whole. The upper panel corroborates the conclusion that the uniform $C_v = 1$ solution is unacceptable: that solution corresponds to τ_v having its minimum value at all velocities, whereas the best-fit optical depth is consistently larger than the minimum.

4.3.3. Broad Ca II Absorption: Velocity Regime A

To model the Ca II 3934 absorption in velocity regime A (4337–5657 km s⁻¹), we extrapolate from the absorption at 4000–4337 km s⁻¹ in velocity regime B. The absorption there, while noisy, is much more consistent with the minimum C_v than with $C_v = 1$, and the optical depth is consistent with being constant at the weighted average optical depth of $\tau_v = 0.88 \pm 0.03$. We adopt a fixed $\tau_v = 0.88$ for regime A, which means that the corresponding fractional absorption in Ca II 3969 is 61% of that in Ca II 3934 and that the covering factor C_v is 1.71 times its minimum possible value at each v . We also calculate the limiting minimum- C_v and $C_v = 1$ cases, as they delimit the range of plausible systematic errors.

4.3.4. Broad Ca II Absorption: Velocity Regime C

To the observed residual Ca II 3934 intensities in this velocity range, we add back in the fractional absorption in high-velocity Ca II 3969 estimated in the previous section. We then solve for C_v and τ_v as per usual. Figure 5 shows the results. The uncertainty ranges shown as the grey areas include the systematic uncertainties arising from the removal of the high-velocity Ca II 3969. Note that the removal of high-velocity Ca II 3969 resulted in a large increase in the number of pixels in this velocity regime with valid physical solutions.

In most velocity bins, the minimum C_v solution cannot be ruled out but the $C_v = 1$ solution can. On average, however, C_v is significantly larger than the required minimum value. This behavior is similar to that in velocity regime B, though not as pronounced.

4.3.5. Broad Ca II Absorption: Summary

Figure 6 shows the optical depth and covering factor over the velocity range of strong Ca II absorption. As mentioned previously, the covering factor is on average significantly greater than the minimum value, though it tracks the minimum value more closely in velocity regime C than in regime B. The Ca II outflow is moderately saturated ($1 < \tau < 3$), with only one significant spike above 4. Thus, in general, the covering factor determines much, but not all, of the shape of the absorption profile in the Ca II outflow.

4.3.6. The Broad Mg I 2852 Absorption

As seen in Figure 3, the strongest Mg I absorption in the broad outflow is present between 2000–3000 km s⁻¹. Figure 7 shows the absorption and Ca II optical depth over this velocity range in detail. Not all the fluctuations in τ_v are likely to be real, but the very high- τ_v features marked with the dotted lines are statistically significant. (The lone high- τ_v feature near 2600 km s⁻¹ is likely a residual from the correction of blended associated absorption in the Ca II 3969 trough.) The two features between 2200–2400 km s⁻¹ have weak Mg I. The three narrow absorption features between 2700–2900 km s⁻¹ have a larger Mg I/Ca II ratio, since they have equal or smaller $\tau_{\text{Ca II}}$ (and similar τ_v) but stronger Mg I absorption.¹⁵

Note that there is no evidence for any features in the (heavily saturated) Mg II trough at these velocities, nor is there any sign of Ca I 4227.9 absorption.) As with the Mg I/Ca II ratio variations in the associated absorber (Appendix A), this seems likely to be due to metallicity or abundance variations, though CLOUDY modeling is needed to firmly rule out an ionization parameter effect. The striking similarity of the features in the Mg I and Ca II troughs rules out the possibility that the two ions are found in physically distinct regions that happen to share the same velocity.

A similar effect may be present in Q 2359–1241. Table 1 of Arav et al. (2001) shows that its absorption component e has a Ca II/Mg I ratio several times larger than that in components b and c. Unlike in SDSS 0300+0048, the broader component (e) has the higher Ca II/Mg I ratio. However, the spectra of Arav et al. (2001) included only one line of the Ca II doublet, so the reality of the Ca II/Mg I variation in Q 2359–1241 remains to be confirmed.

4.3.7. Column Densities in the BAL Outflow

For an ion giving rise to unsaturated and instrumentally well-resolved doublet absorption, the optical depth at velocity v is directly proportional to the column density per unit velocity at v , N_v , which has units of cm⁻² (km s⁻¹)⁻¹ (Savage & Sembach 1991). The total column density (Arav et al. 1999) and its uncertainty, both in units of cm⁻², are then given by

$$N = \sum N_v dv = \sum N_v v = \frac{3.7679 \times 10^{14}}{f_1} \sum \tau_v v; \quad N = \frac{3.7679 \times 10^{14}}{f_1} \frac{\sum \tau_v v}{(\sum v)^2} \quad (12)$$

where we have ignored the uncertainties on the wavelength λ_1 (in Å) and the dimensionless oscillator strength f_1 of the stronger line of the doublet, which has optical depth τ_v in the velocity bin of width Δv (in km s⁻¹) at velocity v .¹⁶ For

¹⁵ The three features are seen in both Mg I and Ca II, but the velocity distributions of their absorption strengths differ in two features. The $\tau_{\text{Ca II}}$ does match the depths of the Mg I features rather well, however, suggesting that Mg I is unsaturated while the large τ_v and variable C_v in Ca II shift its velocity centroid away from that of Mg I.

¹⁶ N and N_v are independent of the covering factor C_v , but the total mass present in that ion along the line of sight does depend on C_v .

saturated absorption, Eq. 12 yields a lower limit to the true N . For a singlet transition with $C_v = 1$, $I_v = I_e v = I_1 = I_1$. At velocities where I_v or I_e are formally undefined, we linearly interpolate using the two nearest defined values. For singlet transitions, for velocities where I_v is formally undefined we assume that $I_v = \ln(I_1)$, even if the result is a negative I_v .

We are interested in the column densities in three different velocity regimes, which are not quite the same as the Ca II regimes ABC. First is 1697–3740 km s⁻¹, where the Ca II absorption is strong but excited Fe II absorption is absent. Next is 3740–5657 km s⁻¹, where both Ca II and excited Fe II absorption are present. Last is 5657–8221 km s⁻¹, where Ca II is absent but Mg II and excited Fe II remain relatively unconfused. The column densities we derive for the various ions in these velocity regimes are listed in Table 1 and are discussed below. We do not measure column density limits for the additional 2600 km s⁻¹ of Mg II and excited Fe II absorption which are present at > 8221 km s⁻¹ (x4.3.1).

We find a total $N_{\text{CaII}} = (7.13 \pm 1.15) \times 10^4 \text{ cm}^{-2}$. For Ca I 4227.9 we assume $C_v = 1$ to set a limit of $N_{\text{CaI}} = 1.7 \times 10^2 \text{ cm}^{-2}$ for the entire outflow.

We set a rough lower limit on N_{MgII} by ignoring Mg II 2803 and summing only Mg II 2796, assuming $C_v = 1$ and thus $I_v = \ln(I_1)$, where I_v is the residual intensity at velocity v . This yields $N_{\text{MgII}} = (6.61 \pm 0.36) \times 10^4 \text{ cm}^{-2}$ (for 1697–8221 km s⁻¹). Normalizing by the strong Fe II emitter continuum shown in Figure 2, which is 2 times larger than the continuum we have assumed, would increase by only $\log(2)$ and N_{MgII} by only 20–25%. However, since the Mg II trough is strongly saturated, the value of N_{MgII} is a lower limit regardless of the continuum chosen.

For Mg I we set a conservative lower limit by assuming $C_v = 1$, normalizing by the dashed line in Figure 3, and summing over $v = 2000$ –4500 km s⁻¹. This yields $N_{\text{MgI}} = (1.73 \pm 0.02) \times 10^5 \text{ cm}^{-2}$. A more liberal estimate, obtained using the normalization shown in Figure 3, yields $N_{\text{MgI}} = (5.66 \pm 0.03) \times 10^5 \text{ cm}^{-2}$ for 1697–5157 km s⁻¹, beyond which Mg I is confused with Mg II. Clearly, the systematic uncertainty in the continuum placement dominates the random uncertainties. Moreover, using the strong Fe II emitter continuum would increase the lower limit on N_{MgI} by $N_{\text{MgI}} = 1.1 \times 10^4 \text{ cm}^{-2}$.

As for excited He I (He I* for short), there is a possible detection of weak (~5% of the continuum), broad He I 3188 absorption, but this line lies atop a broad emission complex and so the continuum normalization is quite uncertain. Also, despite confusion with Ca II 3934, we see no sign of He I 3889 absorption with depth more than 5% of the continuum (Fig. 3), even though its optical depth is three times that of He I 3188. He I 2945 provides no useful constraints since the observed continuum surrounding it is simply too complex to be normalized accurately. It is possible there is saturated He I* absorption from a region with $C_v = 0.05$, but we are most interested in limits on He I* at velocities where Ca II or Mg II absorption is seen, and such absorption has $C_v = 0.05$. To estimate a limit on N_{HeI} , we assume absorption 5000 km s⁻¹ wide with $C_v = 1$, $I_{3188} = 0.02$ and $I_{3889} = 0.06$, which yields $N_{\text{HeI}} = 4.6 \times 10^4 \text{ cm}^{-2}$.

Our upper limit on the excited Fe II column (Fe II* for short) at 1697–3740 km s⁻¹ comes from the non-detection of Fe II 2632, which is a blend of two lines. Using NIST database $g_i f_i$ values for these lines from de Kool et al. (2001), we find $N_{\text{FeII}} = (0.42 \pm 1.62) \times 10^5 \text{ cm}^{-2}$. Our lower limits on the excited Fe II column at higher velocities come from assuming $C_v = 1$ and attributing the absorption to a blend of all Fe II multiplet UV1 lines from 2618–2633 Å, a velocity span of 1600 km s⁻¹. We used NIST database $g_i f_i$ values from de Kool et al. (2001) for those lines also. An exact accounting of which lines contribute at which wavelengths would change the calculated lower limit somewhat, but the saturated absorption means the column density is probably much greater than the lower limit anyway. We do not attempt to convert these limits on the Fe II column in states 0.1 eV above ground to limits on the total Fe II column.

Our column densities could be underestimates if features in the outflow are barely resolved at our velocity resolution. If this is the case, recalculating the column densities after binning the spectrum will yield significantly smaller values. We find this to be only a 10% effect: the Ca II column densities calculated from the spectrum after binning by v pixels are about 15% lower than the unbinned values in velocity regime B and 5% lower in velocity regime C.

5. discussion

5.1. Broad Ca II Absorption vs. Broad, Excited Fe II Absorption

It is worth reiterating the interesting fact that the BAL region responsible for the main Ca II trough also produces Mg I and Mg II absorption, but none from excited Fe II except at the highest velocities where Ca II is seen (x4.3.1 and Fig. 3). Presumably the Ca II region does produce ground-state Fe II absorption, but such absorption cannot be studied since it is blended with higher-velocity excited Fe II.

Since the true continuum at the wavelengths where we expect to see excited Fe II absorption from the Ca II-absorbing gas is likely much higher than we have assumed (Fig. 2), there is almost certainly some absorption present at those wavelengths. Nonetheless, we can rule out the possibility that excited Fe II is present at 2000–3500 km s⁻¹ with nonblack saturation. For that to be the case, the unabsorbed continuum at the velocities in question would have to be higher than we have assumed by a factor equal to the inverse of the partial covering. The Ca II absorber reaches $C_v = 0.95$ in this velocity range. Thus the unabsorbed continuum would have to be twenty times higher, whereas only a factor of two difference is expected at rest 2600 Å even if the true continuum is that of a strong Fe II emitter (Fig. 2).

One possible explanation for the different velocity distributions of Ca II and excited Fe II is that the Ca II region has a density too low for collisional excitation to significantly populate excited states of Fe II ($n_e < 10^3 \text{ cm}^{-3}$; de Kool et al. 2001); radiative excitation will not contribute significantly at such densities either (x4.1.3 of Wampler, Chugai, & Petitjean 1995). Alternatively, the Ca II could arise from a region with a density similar to that in the Fe II region, but with a lower temperature. The levels which give rise to Fe II 2632 absorption have an average excitation potential of 0.095 eV, so a temperature $T \sim 1100 \text{ K}$ is required to avoid populating them significantly. Absorption from the somewhat

weaker Fe II 2626 line is not detected either, and its excitation potential is only 0.048 eV. Thus the temperature could be as low as $T \sim 550$ K in the Ca II region. Which of these alternatives – low density or low temperature – is most likely the case for the Ca II region depends on the structure of the outflow, as we now discuss.

5.2. Column Densities and Outflow Models

Compared to Q 2359–1241 (Arav et al. 2001), the only other Ca II BAL quasar studied at high resolution, SDSS 0300+0048 has lower limits on the total Mg I and Mg II column densities – 30 times larger, a lower limit on the excited Fe II column – 95 times larger, an upper limit on the excited He I column – 8 times larger, and a total Ca II column – 200 times larger. The column densities for all but the excited Fe II are the largest reported to date in any BAL outflow.

These values are consistent with the total column density of metals being – 200 times larger in SDSS 0300+0048 than in Q 2359–1241. The excited He I column need not increase as much because it comes from the He II region instead of the low-ionization BAL region which produces most of the absorption in SDSS 0300+0048. Also, the excited He I absorption can be greatly reduced if the He II region has an n_e below the critical density for this excited state ($3 \times 10^8 \text{ cm}^{-3}$).

Arav et al. (2001) found that the absorption in Q 2359–1241 could be explained by solar metallicity gas with $\log N_H \sim 20$ and $\log U \sim 3$. The existence of a hydrogen ionization front requires a column density $N_H \sim U \times 10^{23} \text{ cm}^{-2}$, or a few times larger for electron densities $n_e \sim 10^{9.5} \text{ cm}^{-3}$ (Davidson & Netzer 1979; de Kool et al. 2002a). Q 2359–1241 has just enough column density to have a hydrogen ionization front (~ 2.5 at the Lyman limit). The 200 times greater Ca II column density in SDSS 0300+0048 means that it must have a strong hydrogen ionization front. Even if SDSS 0300+0048 is one of the most metal-rich quasars known, with metallicity ~ 15 times solar (Baldwin et al. 2002), it would have to have a Ca II region with 13 times larger N_H than Q 2359–1241, corresponding to ~ 33 at the Lyman limit.

The presence of an H I ionization front in SDSS 0300+0048 agrees with expectations from photoionization calculations (Ferland & Persson 1989). An H I ionization front surrounding the quasar¹⁷ can shield Mg II and Fe II from ionization (Voit, Weymann, & Korista 1993), but by itself cannot protect Mg I or Ca II. Since those ions have lower ionization potentials than H I, they are only found where the ionization parameter is low (Hamann et al. 2001). Mg I can be found in low-ionization gas with column density less than, or just equal to, that needed for an H I ionization front (Arav et al. 2001). Ca II cannot, due to resonant photoionization from the lowest metastable level of Ca II by Ly photons (Joly 1989). Thus, in practice, Ca II only exists outside an H I front where both the ionization parameter and the Ly photon density are low.

The excited Fe II BAL region cannot be farther from the quasar than the Ca II BAL region. If it was, it would lie outside the H I ionization front and would also show Ca II strong absorption. (The weak Ca II absorption from the excited Fe II region means that at most $\sim 10\%$ of the excited Fe II-absorbing gas could lie outside the front.) This fact, along with the observations that the broad absorption is detached from the system redshift and that the Ca II BAL region lies at low velocities ($1697\text{--}3740 \text{ km s}^{-1}$) while the excited Fe II BAL region lies at high velocities ($3740\text{--}8221 \text{ km s}^{-1}$ and beyond), enable us to constrain which of two competing BAL outflow models might explain SDSS 0300+0048. These models are the disk wind model of Murray et al. (1995) and a model where the absorption arises in connected clouds embedded with very small filling factor in a less dense, hotter medium (e.g., Arav & Li 1994). Such clouds could form a dusty outflow which nearly surrounds the quasar (e.g., Becker et al. 2000), or they could be ‘ablated’ from denser sources (such as an accretion disk or obscuring torus) and only block some lines of sight to the quasar.

In the radiatively driven disk wind model of Murray et al. (1995), the streamlines of the outflow begin at some angle to the disk and then bend to become asymptotically radial (in cross-section). Thus the detachment velocity simply reflects the height above the disk reached by the flow before it crosses the line of sight to the continuum source, which could be different for different ions. As the distance from the quasar increases along a single streamline, the velocity and ionization increases and the density decreases. For two streamlines arising at different radii, the more distant streamline will be scaled up in density but down in velocity and ionization parameter. Our line of sight crosses numerous streamlines, so we expect to see higher-velocity gas which is less dense, more highly ionized, and at smaller radii.¹⁸

The BAL outflow in SDSS 0300+0048 is consistent with such a disk wind, as the lowest-ionization gas (traced by Ca II and Mg I) is found at the lowest velocities.¹⁹ To be consistent with the observed anticoincidence of excited Fe II absorption and Ca II absorption requires that a disk wind in SDSS 0300+0048 have $n_e > 10^3 \text{ cm}^{-3}$ throughout but $T \sim 1100$ K at the low velocities (large radii) where Ca II is present. If the velocity decreases monotonically with radius along the line of sight, then the H I ionization front will shield gas at all velocities less than some velocity v_s . Since the Ca II absorption can only arise outside the H I ionization front, we assume either that $v_s \sim 5750 \text{ km s}^{-1}$, which is the maximum observed Ca II velocity, or that $v_s \sim 4000 \text{ km s}^{-1}$, which divides strong and weak Ca II absorption, and that the higher-velocity Ca II absorption is due to a small portion (by mass) of the outflow departing from a monotonically decreasing velocity. If the Mg II trough were not saturated, it might reveal the velocity of the front, as the ionic fraction of Mg II increases sharply outside the front (Voit et al. 1993).

¹⁷ The ionization front is centered on the quasar, so we use the terms inside and outside the front instead of in front of and behind the front.

¹⁸ The simulations of Proga, Stone, & Kallman (2000) verify these analytic predictions of Murray et al. (1995) for radiatively driven disk winds. These predictions are less secure in the magnetohydrodynamic simulations of Proga (2003), which yield a turbulent zone of considerable solid angle between the fast radiatively-driven wind component and a slower MHD component which develops closer to the equatorial plane. Should the line of sight pierce that latter zone, the relationship between velocity, density, ionization parameter and distance may break down.

¹⁹ The same may be true for FBQS 1044+3656, where the Ca II absorption is found at the low-velocity end of that object’s higher-velocity outflow (White et al. 2000; de Kool et al. 2001). However, note that the velocity distributions are the same for Ca II and excited Fe II in Q 2359–1241 (Arav et al. 2001) and Mrk 231 (Smith et al. 1995; Rupke et al. 2002).

If we try to explain the Ca II absorption as arising from clouds with a lower density than the clouds giving rise to excited Fe II absorption, but at similar radii, then the Ca II BAL clouds must have $n_e < 10^3 \text{ cm}^{-3}$ while the excited-Fe II BAL clouds have a higher n_e and lower T , assuming all clouds are in pressure balance with the same confining medium. But the column density in the Ca II clouds must be larger than that in the excited-Fe II BAL clouds, which leads to an improbable scenario where large, diffuse clouds extend to high column densities but small, dense clouds do not. Thus, as in the disk wind case, we are driven to a scenario where the excited Fe II BAL clouds must have $n_e > 10^3 \text{ cm}^{-3}$ while the Ca II BAL clouds have an even higher n_e but a temperature $T \lesssim 1100 \text{ K}$, to avoid populating the excited Fe II levels.

For a cloud scenario where the outflow surrounds the quasar, the outflow must have smaller velocities at larger radii because the Ca II BAL region must lie at larger radii than the excited Fe II BAL region. This might occur if this quasar recently ‘turned on’ inside a relatively thick shell or torus of gas, and has gradually radiatively accelerated it such that the velocity in the shell is a decreasing function of radius. The Ca II absorption would arise in the outermost regions of the outflow, which have only been accelerated to velocities of $\sim 2000\text{--}4000 \text{ km s}^{-1}$ so far. This scenario is rather contrived, especially since such an outflow will be Rayleigh-Taylor unstable (though magnetic fields might suppress the instabilities), but it can be tested by looking for a long-term increase in the velocity of the Ca II BAL outflow.

A cloud scenario where the outflow does not surround the quasar can explain the detached troughs by positing that the injection points of the clouds (where they have $v_{\text{radial}} = 0$) do not lie along our line of sight to the continuum source, and that there is some finite outer radius for the injection which corresponds to the minimum radial velocity we observe. Thus the outflow cannot be spherically symmetric, as such a flow would have injection points along all lines of sight. Injection of clouds from a disk or torus is still feasible. The clouds must cross our line of sight in a spatially- and velocity-segregated flow, as in the disk wind case, because the (low-velocity) Ca II-absorbing clouds must be at larger radii than the (high-velocity) Fe II-absorbing clouds. If clouds of all velocities were intermixed, the gas in any high-velocity clouds shadowed by a low-velocity Ca II-absorbing cloud would recombine to lower ionization states on timescales of $\sim 10^1/n_e$ seconds. The result would be Ca II absorption at high velocities as well as low, which is not seen.

Thus, for a cloud model to explain this outflow the clouds must form either a rather contrived expanding shell or a segregated flow of clouds arising from a disk or torus. The latter case differs from the disk wind model only in the presence of a hot, confining medium for the clouds.

Finally, it is not clear how the associated absorption fits in to either the cloud or the disk wind model. However, in both models it must arise far enough from the continuum source that it has not been significantly accelerated. Another of the few overlapping-trough BAL quasars in H 02, SDSS 0819+4209, has BAL troughs detached from an AAL system. That object has a similar detachment velocity ($v = 2180 \pm 80 \text{ km s}^{-1}$), though the Mg II AAL appears to be broader than in SDSS 0300+0048. Anecdotally, AALs and detached BALs appear to be common in additional overlapping-trough quasars being found by the SDSS, but the possible significance of this finding to models of these outflows remains unclear.

6. conclusion

Comparison with Q 2359–1241, the only other Ca II BAL quasar studied at high resolution, suggests that the outflow in SDSS 0300+0048 has a strong H I ionization front, in agreement with the photoionization modeling of Ca II by Ferland & Persson (1989). The observed Ca II absorption must arise in low-ionization gas located outside the ionization front.

Kinematically, the outflow is detached – it only begins at a velocity blueshifted by $\sim 1700 \text{ km s}^{-1}$ from the associated absorption redshift. Furthermore, excited Fe II absorption is seen only at high velocities, and strong Ca II absorption only at the low velocity end of the outflow.

The velocity and ionization structure in SDSS 0300+0048 can be explained in a disk wind model where the Ca II arises only at large radii. A cloud model for the BAL outflow can explain the observations if the clouds form a segregated flow originating from a source out of our line of sight; in other words, a clumpy disk wind instead of a smooth one (e.g., Everett 2003). An outflow of clouds which completely surrounds the quasar can explain the observations only in the case of a shell of gas in which the velocity decreases with increasing radius and in which the gas has been uniformly accelerated such that none of it has velocities $v \lesssim 1700 \text{ km s}^{-1}$. While somewhat contrived, this model is testable since it predicts a long-term increase in the observed velocity of the outflow.

The region producing excited Fe II absorption must have $n_e > 10^3 \text{ cm}^{-3}$ and $T \gtrsim 1100 \text{ K}$ to significantly populate the observed fine structure levels. In any of these models, it is almost certain that the region producing Ca II absorption also has $n_e > 10^3 \text{ cm}^{-3}$, in which case the Ca II-absorbing region must have $T \lesssim 1100 \text{ K}$ – and perhaps as low as $T \lesssim 550 \text{ K}$ – to prevent excited Fe II states from being populated there.

More generally, quasars with detached Ca II troughs (and thus an H I ionization front) enable a test of the disk wind model prediction of a monotonically decreasing velocity with increasing radius. Since the lowest velocity absorption arises outside the front, no high-ionization gas should be present at the lowest velocities. This test cannot be made in SDSS 0300+0048 since Fe II absorption obliterates the spectrum. It might be possible using spectra covering C iv in Ca II LoBALs with narrower troughs, such as FBQS 1044+3656. However, the disk wind model does not explain Q 2359–1241. In that object, weak Ca II absorption is found at the same velocity as excited He I absorption (which traces the high-ionization He II column) and N v absorption is seen at lower velocities than Ca II, though the C iv absorption is mostly at higher velocities (Arav et al. 2001). If the Q 2359–1241 outflow is a disk wind, it is more complicated than the analytic disk wind model of Murray et al. (1995).

The associated absorption line system in SDSS 0300+0048 (Appendix A) exhibits partial covering, and therefore is likely located near the central engine. Whether or not it is associated with the BAL outflow is unclear. Blending of the

AAL with the BAL trough shows that the spatial regions covered by the BAL outflow varies over velocity differences of 1700 km s^{-1} . Variations in the Mg I/Ca II ratio with velocity are also seen in both the BAL and AAL systems; these appear more likely to be due to variations in metallicity or abundances than in the ionization parameter.

In conclusion, in H02 we stated that "targeted high resolution spectroscopy of Ca II in SDSS 0300+0048 ... might determine if the column densities as well as the outflow velocities are very large." We have shown herein that the BAL outflow column densities are among the largest yet measured in BAL outflows. Furthermore, the highly ionized gas columns are as yet largely unconstrained. Upcoming Chandra and possibly XMM-Newton observations will be able to constrain the total BAL column density regardless of ionization state.

We thank F. Barrientos, C. Churchill, I. Strateva and J. Veliz. P.B.H. acknowledges financial support from Chilean grant FONDECYT/1010981 and from Fundacion Andes. Funding for the creation and distribution of the SDSS Archive has been provided by the Alfred P. Sloan Foundation, the Participating Institutions, the National Aeronautics and Space Administration, the National Science Foundation, the U.S. Department of Energy, the Japanese Monbukagakusho, and the Max Planck Society. The SDSS Web site is <http://www.sdss.org/>. The SDSS is managed by the Astrophysical Research Consortium (ARC) for the Participating Institutions. The Participating Institutions are The University of Chicago, Fermilab, the Institute for Advanced Study, the Japan Participation Group, The Johns Hopkins University, Los Alamos National Laboratory, the Max-Planck-Institute for Astronomy (MPIA), the Max-Planck-Institute for Astrophysics (MPA), New Mexico State University, University of Pittsburgh, Princeton University, the United States Naval Observatory, and the University of Washington. This research has made use of the Atomic Line List v2.04 at <http://www.pa.uky.edu/~peter/atomic/>.

APPENDIX

the associated absorption

We are interested primarily in the broad Ca II absorption, but there is narrow associated Ca II 3934 blended with the broad Ca II 3969. To remove this absorption we must model the associated system.

To determine the continuum around each absorption line from the associated absorber, we make the simplifying assumption that the associated absorption is external to the broad absorption line region, an assumption we reconsider at the end of this section. Under this assumption, the locally measured continuum around each line is a good estimate of the true continuum seen by the associated absorber. Since there is structure near the associated Mg II which appears to be due to additional weak Mg II emission or absorption, we construct a local continuum for the associated Mg II by fitting a single polynomial continuum, offset only by a small flux difference, to both transitions in velocity space.

Figure 8 shows that the associated system is seen in Ca II, Mg II, Mg I, Fe II 2600, Fe II 2382 (and Fe II 2374, which is not plotted), but not in Fe II 2586. We will return to this point at the end of this section. Ca II 3969 and Mg I absorption are both weaker than Fe II 2600 absorption, but their profiles are broadly consistent with the Fe II 2600 absorption profile seen at lower optical depths. Since both ions exist only in gas with a low ionization parameter, they should show the same covering factors if they are saturated. We conclude that the Ca II and Mg I absorption lines are unsaturated, with different v . Overall, the associated absorption appears to have a higher Mg I/Ca II ratio than the broad absorption does ($\times 4.3.1$). Also, within the associated absorption itself, the subsystem at $\sim 32 \text{ km s}^{-1}$ has a noticeably higher Mg I/Ca II ratio. This fact suggests the existence of inhomogeneities in the ionization, metallicity, or relative abundances as a function of velocity in the associated absorber (Churchill et al. 2002, and references therein).

We can use the unsaturated associated Ca II 3969 absorption to model the optical depth in associated Ca II 3934, but the Mg II absorption indicates that the associated absorber exhibits partial covering of the continuum source. Even though Mg II can occur in somewhat higher ionization gas than Ca II can, we can do no better than to assume that the associated Ca II has the same partial covering with velocity as Mg II.

The results of using Eqs. 3-4 to compute C_v and v for Mg II are shown in Figure 9. The absorber has $v \sim 1$ at almost every velocity. The observations are not quite consistent with $C_v = 1$ at all velocities: C_v appears lower at $v > 10 \text{ km s}^{-1}$ than at $v < 10 \text{ km s}^{-1}$. Since the relative C_v of Ca II and Mg II are somewhat uncertain, and since the observed variations in C_v are consistent with the random noise, we will approximate C_v as a step function. From ~ 54 to 10.5 km s^{-1} we find an average partial covering of $C = 0.93 \pm 0.04$ (with $M_{\text{gII}} \sim 7$). From 10.5 to 64 km s^{-1} we find an average partial covering of $C = 0.76 \pm 0.09$ (with $M_{\text{gII}} \sim 3$). There is additional absorption from 64 to about 93 km s^{-1} for which the C breaks down because the 2796Å absorption is less than half the strength of the 2803Å absorption. It is likely that our continuum fit is in error at these velocities in one or both of the Mg II lines.

We now apply these two covering factors to the associated Ca II 3969 absorption to predict the optical depth of the associated Ca II 3934 absorption. If the associated absorption is external to the broad absorption, then independent of any assumption about the true continuum incident on the broad absorption line region the flux corrected for the associated Ca II 3934 absorption F is related to the observed flux O by

$$O = F [1 - C(1 - e^{-R})] \quad (\text{A1})$$

where τ is the optical depth in Ca II 3969 and all quantities except R are functions of velocity. Since we know O and R , and have estimates for C and τ_{3969} , we can recover F . Figure 10 shows the spectral region around associated Ca II 3934 before (solid) and after (dashed) this correction. The corrected spectrum appears reasonable everywhere except for a narrow spike near $\sim 53 \text{ km s}^{-1}$, which is interpolated over for our analysis.

Associated or Broad Absorption: Which Comes First?

Because the associated Ca II 3934 spans such a narrow velocity range, our correction for it is not critical to the subsequent analysis of the BAL trough. Nonetheless, before proceeding it is worth considering further our assumption that the associated absorption arises outside the broad absorption line region. The probable partial covering of the associated absorber immediately calls into question this assumption, since partial covering is seen almost exclusively in gas linked with the central engines of AGN. However, while we cannot rule out a close connection between the associated and broad absorbers, we now show that neither can we rule out that the associated absorption arises near the nucleus but external to the broad absorption region.

The key insight comes from considering the associated absorption in Fe II 2374,2382 and Fe II 2586,2600, lines that all arise from the lowest *n*-structure level in the ground term of Fe II. Between the redshifted wavelengths of the associated Fe II 2600 and Fe II 2586, the excited Fe II UV1 BAL removes most of the continuum, but not quite all (Figure 1). If the associated absorption arises far out in the quasar host galaxy, we might expect to see Fe II 2586 absorb 93% of the remaining continuum, just as Fe II 2600 does. The normalized flux and 1 σ uncertainties in this spectral region are shown in the second panel from the bottom of Figure 8. Although the noise is large, there is no evidence for the expected absorption even when the spectrum is binned. However, there is clear evidence for Fe II 2382 absorption (Figure 8, bottom panel). This spectral region is equally noisy, but in this case the absorption is consistent with being 93% of the surrounding continuum.²⁰ The same is true for Fe II 2374, while the Fe II 2344 region is too noisy for analysis.

The apparent lack of Fe II 2586 absorption rules out the simple picture of a BAL trough and an associated absorption line system (AAL) which each absorb spatially fixed regions of quasar emission, shown schematically in the top panel of Figure 11. This conclusion applies even if the BAL or AAL regions are not well characterized by a single C and δ (de Kool et al. 2002b). To explain our observations requires some variation with velocity in the quasar emission region covered by the BAL trough. The bottom panel of Figure 11 is a sketch of this spatially distinct, velocity-dependent partial covering.

The reason the BAL region can partially cover spatially distinct emission regions at the wavelengths of the two associated Fe II transitions is that the broad Fe II absorption includes absorption from excited *n*-structure levels, while the narrow Fe II absorption arises from only the ground level. At the zero-velocity wavelength of associated Fe II 2382, the broad Fe II absorption can be approximated as having some velocity v_1 . Since it consists of absorption in different Fe II multiplet UV2 transitions at different velocities, $v_1 = \frac{1}{N} \sum_i w_i v_i$, where w_i is the relative strength of line *i* at velocity v_i . Similarly, at the zero-velocity wavelength of associated Fe II 2586, the broad Fe II absorption will consist of Fe II multiplet UV1 transitions and can be approximated as having velocity $v_2 = \frac{1}{M} \sum_j w_j v_j$. The velocities v_1 and v_2 will be similar but not identical. In SDSS 0300+0048, that velocity difference allows the associated and broad Fe II absorbers to overlap the same spatial region at the wavelength of associated Fe II 2586 but not at the wavelength of associated Fe II 2382. There must be considerable variation in the regions being partially covered over velocity differences of only 1700 km s⁻¹, but similar effects have been seen before in FBQS 1408+3054 ($\times 6.12$ of H02) and NGC 3783 (Gabel 2002).

We cannot prove that the associated absorber is external to the BAL region, but we have shown that such a geometry, coupled with the spatially distinct, velocity-dependent partial covering that must be present, can explain our observations. We therefore used this 'external' assumption to remove the associated Ca II absorption from the broad Ca II trough.

REFERENCES

- Ara, N., Brotherton, M. S., Becker, R. H., Gregg, M. D., White, R. L., Price, T., & Hack, W. 2001, *ApJ*, 546, 140
- Ara, N., Korista, K. T., de Kool, M., Junkkarinen, V. T., & Begelman, M. C. 1999, *ApJ*, 516, 27
- Ara, N. & Li, Z. 1994, *ApJ*, 427, 700
- Baldwin, J. A., Hamann, F., Korista, K. T., Ferland, G. J., Dietrich, M., & Warner, C. 2002, *ApJ*, in press (astro-ph/0210153)
- Becker, R. H., White, R. L., Gregg, M. D., Brotherton, M. S., Laurent-Muehleisen, S. A., & Ara, N. 2000, *ApJ*, 538, 72
- Blanton, M. R., Lupton, R. H., Maley, F. M., Young, R., Zehavi, I., & Loveday, J. 2003, *AJ*, in press (astro-ph/0105535)
- Boroson, T. A. & Green, R. F. 1992, *ApJS*, 80, 109
- Branch, D., Leighly, K. M., Thomas, R. C., & Baron, E. 2002, *ApJ*, 578, L37
- Churchill, C. W., Mellon, R. R., Charlton, J. C., & Vogt, S. S. 2002, *ApJ*, submitted (astro-ph/0212120)
- Davidson, K. & Netzer, H. 1979, *Reviews of Modern Physics*, 51, 715
- de Kool, M., Ara, N., Becker, R. H., Gregg, M. D., White, R. L., Laurent-Muehleisen, S. A., Price, T., & Korista, K. T. 2001, *ApJ*, 548, 609
- de Kool, M., Becker, R. H., Ara, N., Gregg, M. D., & White, R. L. 2002a, *ApJ*, 570, 514
- de Kool, M., Korista, K. T., & Ara, N. 2002b, *ApJ*, 580, 54
- Everett, J. E. 2003, *ApJ*, submitted (astro-ph/0212421)
- Fan, X., Strauss, M. A., Gunn, J. E., Lupton, R. H., Carilli, C. L., Rupen, M. P., Schmidt, G. D., Moustakas, L. A., et al. 1999, *ApJ*, 526, L57
- Ferland, G. J. & Persson, S. E. 1989, *ApJ*, 347, 656
- Fukugita, M., Ichikawa, T., Gunn, J. E., Doi, M., Shimazaki, K., & Schneider, D. P. 1996, *AJ*, 111, 1748
- Gabel, J. R. et al. 2002, *ApJ*, in press (astro-ph/0209484)
- Ganguly, R., Eracleous, M., Charlton, J. C., & Churchill, C. W. 1999, *AJ*, 117, 2594
- Graham, M. J., Clowes, R. G., & Campanano, L. E. 1996, *MNRAS*, 279, 1349
- Gunn, J. E., Carr, M., Rockosi, C., Sekiguchi, M., Berry, K., Elm, S. B., de Haas, E., Ivezić, Z., et al. 1998, *AJ*, 116, 3040
- Hall, P. B., Anderson, S. F., Strauss, M. A., York, D. G., Richards, G. T., Fan, X., Knapp, G. R., Schneider, D. P., et al. 2002, *ApJS*, 141, 267 (H02)
- Hall, P. B. & Hutsemekers, D. 2003, to appear in *Active Galactic Nuclei, from Central Engine to Host Galaxy*, eds. S. Collin, F. Combes and I. Schmalan, in press (astro-ph/0211089)
- Hamann, F., Barlow, T. A., Chaffee, F. C., Foltz, C. B., & Weymann, R. J. 2001, *ApJ*, 550, 142
- Hamann, F., Barlow, T. A., Junkkarinen, V., & Burbidge, E. M. 1997, *ApJ*, 478, 80
- Hogg, D. W., Finkbeiner, D. P., Schlegel, D. J., & Gunn, J. E. 2001, *AJ*, 122, 2129
- Home, K. 1986, *PASP*, 98, 609
- Joly, M. 1989, *A & A*, 208, 47
- Kwan, J., Cheng, F., Fang, L., Zheng, W., & Ge, J. 1995, *ApJ*, 440, 628
- Lupton, R. H., Gunn, J. E., & Szalay, A. S. 1999, *AJ*, 118, 1406

²⁰ The local continuum used to normalize the Fe II 2586 region in Figure 8 is identical to that used for Fe II 2600: it is at λ_F at the level of the spectrum just longward of Fe II 2600. This same continuum was used to normalize the Fe II 2382 region, for lack of anything better. However, the normalization does not affect the interpretation of why associated absorption from Fe II 2586 was not detected.

- Murray, N., Chiang, J., Grossman, S.A., & Voit, G.M. 1995, *ApJ*, 451, 498
- Pier, J.R., Mun, J.A., Hindsley, R.B., Hennessy, G.S., Kent, S.M., Lupton, R.H., & Ivezić, Z. 2003, *AJ*, in press
- Proga, D. 2003, *ApJ*, in press (astro-ph/0210642)
- Proga, D., Stone, J.M., & Kallman, T.R. 2000, *ApJ*, 543, 686
- Richards, G.T., Fan, X., Newberg, H.J., Strauss, M.A., Vanden Berk, D.E., Schneider, D.P., Yanny, B., Boucher, A., et al., 2002, *AJ*, 123, 2945
- Rupke, D.S., Veilleux, S., & Sanders, D.B. 2002, *ApJ*, 570, 588
- Savage, B.D. & Sembach, K.R. 1991, *ApJ*, 379, 245
- Sigut, T.A.A. & Pradhan, A.K. 2002, *ApJ*, in press (astro-ph/0206096)
- Smith, J.A., Tucker, D.L., Kent, S., Richmond, M.W., Fukugita, M., Ichikawa, T., Ichikawa, S., Jorgensen, A.M., et al., 2002, *AJ*, 123, 2121
- Smith, P.S., Schmidt, G.D., Allen, R.G., & Angel, J.R.P. 1995, *ApJ*, 444, 146
- Srianand, R. & Shankaranarayanan, S. 1999, *ApJ*, 518, 672
- Stoughton, C., Lupton, R.H., Bernardi, M.B., Blanton, M.R., Burles, S., Castander, F.J., Connolly, A.J., Eisenstein, D.J., et al., 2002, *AJ*, 123, 485
- Verner, E.M., Verner, D.A., Korista, K.T., Ferguson, J.W., Hammer, F., & Ferland, G.J. 1999, *ApJS*, 120, 101
- Vestergaard, M. & Wilkes, B.J. 2001, *ApJS*, 134, 1
- Voit, G.M., Weymann, R.J., & Korista, K.T. 1993, *ApJ*, 413, 95
- Wampler, E.J., Chugai, N.N., & Petitjean, P. 1995, *ApJ*, 443, 586
- Weymann, R.J., Morris, S.L., Foltz, C.B., & Hewett, P.C. 1991, *ApJ*, 373, 23
- White, R.L., Becker, R.H., Gregg, M.D., Laurent-Muehleisen, S.A., Brotherton, M.S., Impey, C.D., Petry, C.E., Foltz, C.B., et al., 2000, *ApJS*, 126, 133
- York, D.G., Adelman, J., Anderson, J.E., Anderson, S.F., Annis, J., Bahcall, N.A., Bakken, J.A., Barkhouser, R., et al., 2000, *AJ*, 120, 1579

Table 1
Column Densities in the SDSS J0300+0048 BAL Outflow

Velocity Range:	1697–3740 km s ^{−1}			3740–5657 km s ^{−1}			5657–8221 km s ^{−1}			Total			
Fe II*	(0.04	0.16)	10 ⁵	(1.34	0.09)	10 ⁵	(2.95	0.58)	10 ⁵	(4.29	0.59)	10 ⁵	
Mg II	(1.90	0.34)	10 ⁵	(2.51	0.09)	10 ⁵	(2.20	0.07)	10 ⁵	(6.61	0.36)	10 ⁵	
Mg I	(1.54	0.02)	10 ^{3a}	(2.84	0.02)	10 ³	(4.38						0.03) ^{3a} 10
He I*	2.5		10 ⁴	2.3		10 ⁴	3.1		10 ⁴	7.9			10 ⁴
Ca II	(5.22	0.75)	10 ⁴	(1.91	0.87)	10 ⁴	(0.3	1.2)	10 ²	(7.13	1.15)	10 ⁴	
Ca I	0.2		10 ²	0.8		10 ²	0.7		10 ²	1.7			10 ²

^aThis Mg I column density is a conservative lower limit; more liberal assumptions yield almost exactly the same column density as at 3740–5657 km s⁻¹. In that case, the total Mg I column would be (5.66 ± 0.03) × 10³.

Note. | All column densities are given in units of cm⁻². The asterisks denote ions whose column densities are measured in excited states rather than the ground state.

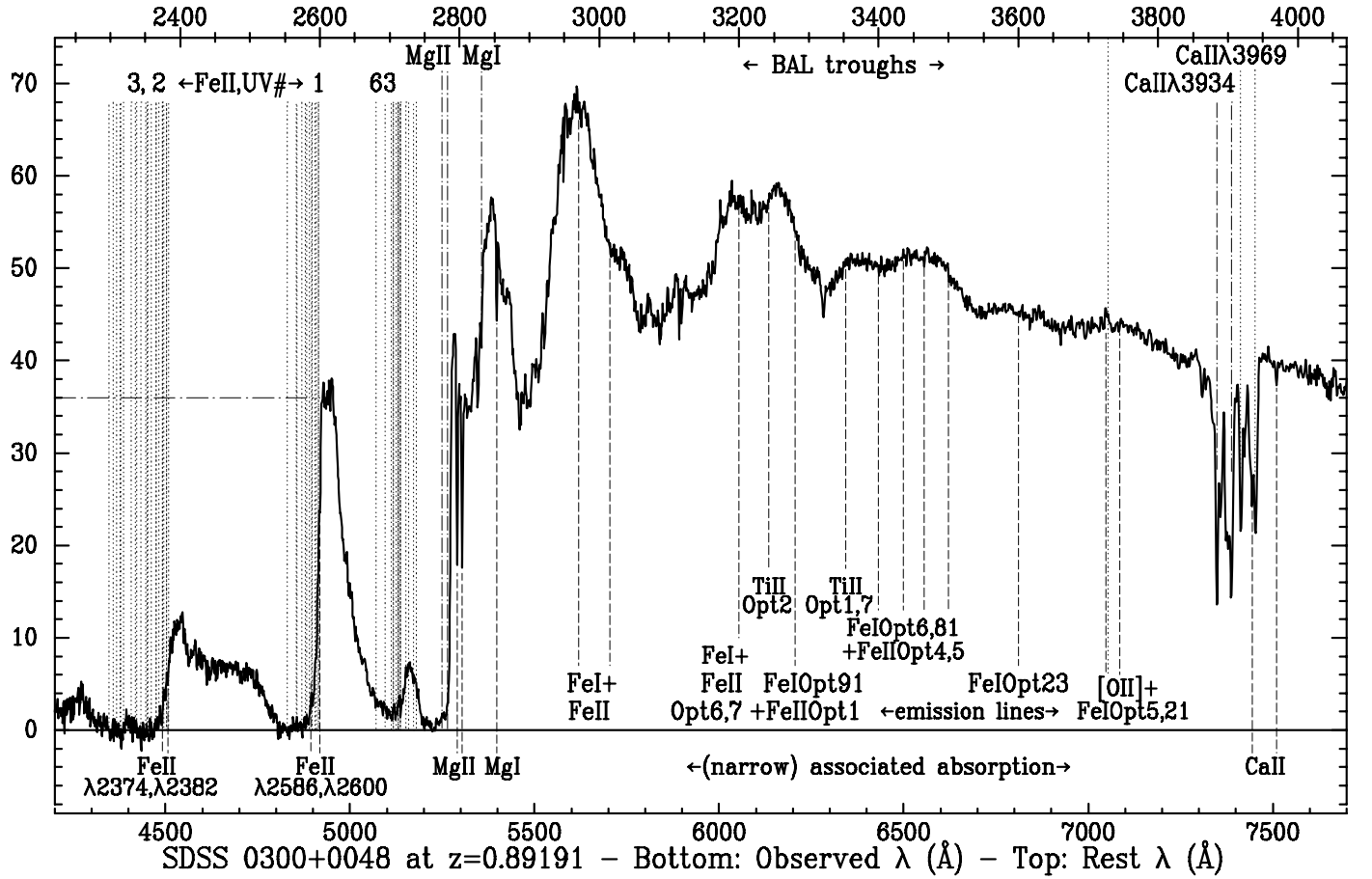


Fig. 1. A portion of the SDSS spectrum ($R=1900$) of SDSS 0300+0048 (F vs.). The broad absorption line troughs are labelled along the top, and the narrow associated absorption lines along the bottom, to help place the UVES spectrum in context. The likely emission lines are labelled just above the labels for associated absorption. The horizontal dot-dashed line shows the continuum level used to normalize the UVES spectrum shortward of 2600 Å rest-frame.

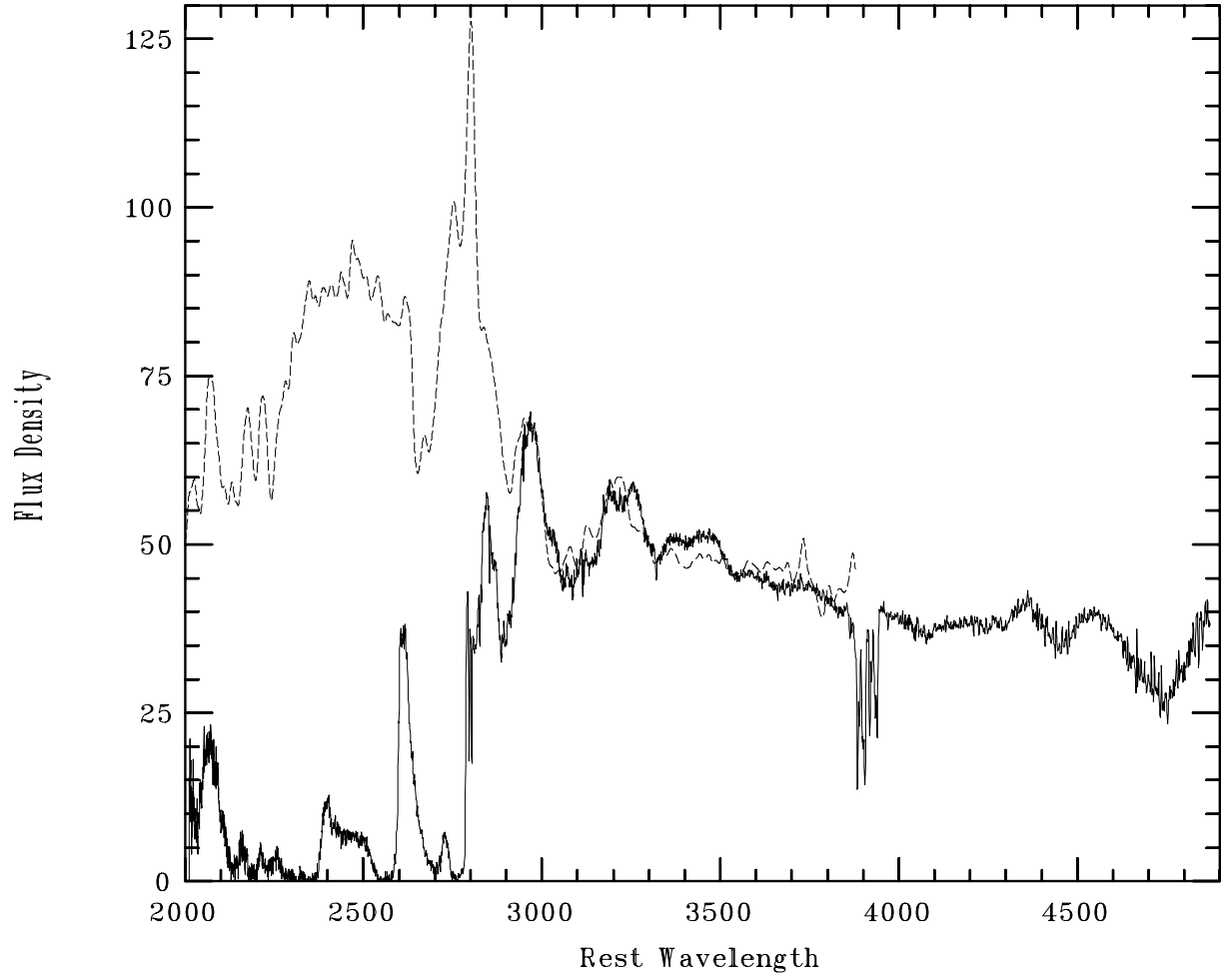


Fig. 2. Flux density (F_{λ}) of SDSS 0300+0048 (solid line) and a model for its intrinsic continuum (dashed line; $\times 4.1$).

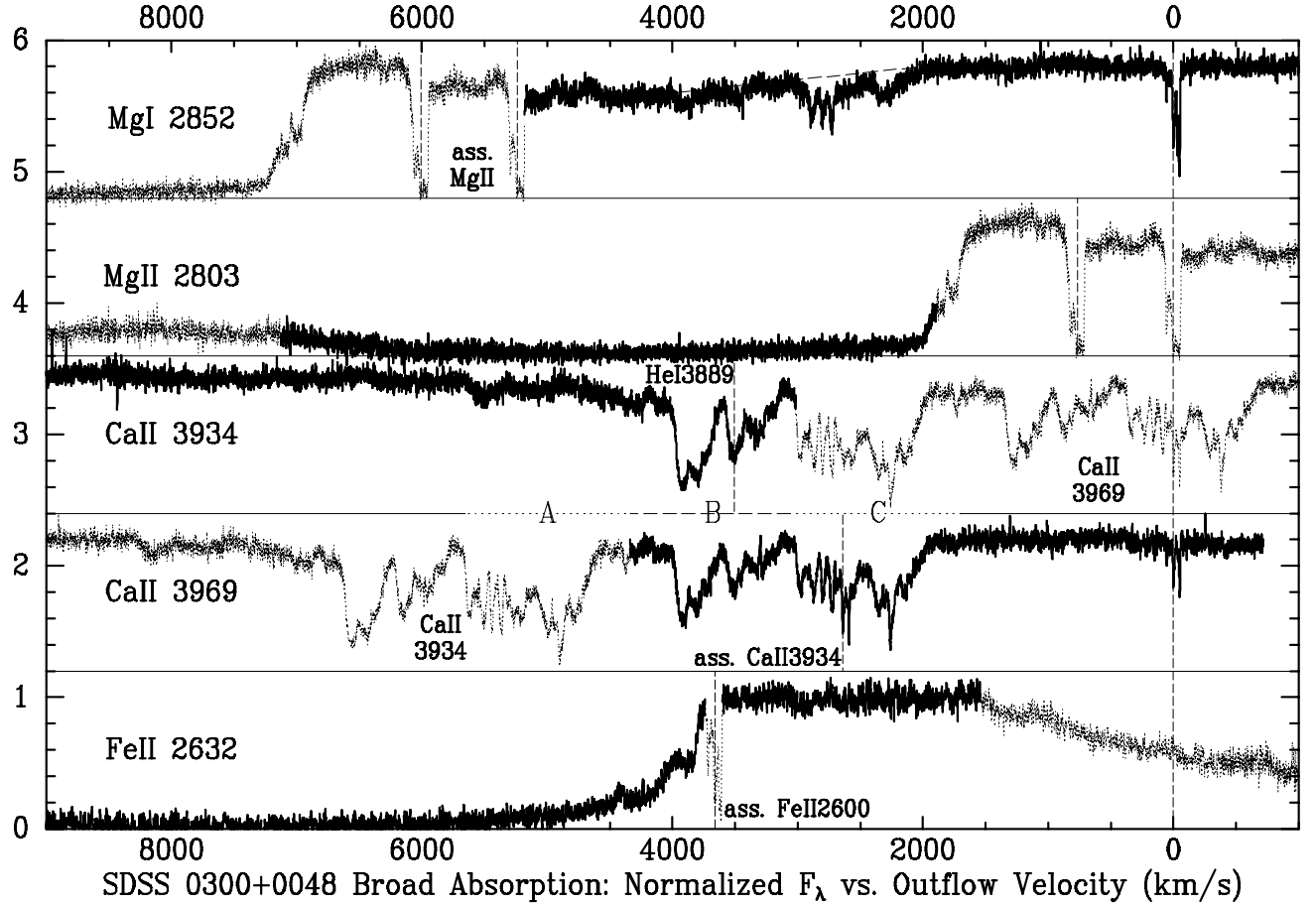


Fig. 3. The normalized spectrum of SDSS 0300+0048 around the broad absorption troughs of five separate transitions. The spectrum of each transition is offset 1.2 units vertically from the one below it, with the thin solid lines showing the zero levels for each transition. Unconfused regions of the spectrum in each transition are shown with heavy lines. The velocity zeropoint is taken to be the redshift of the central component of the associated absorption system, and outflowing velocities are positive; thus, shorter wavelengths appear on the left. Velocity regions A, B and C are indicated between the Ca II 3934 and Ca II 3969 panels (see §4.3). Dashed vertical lines show the locations of associated absorption; note that Fe II 2600 but not Fe II 2632 is seen in the associated absorber. The tilted dashed line in the Mg I panel shows an alternate continuum normalization.

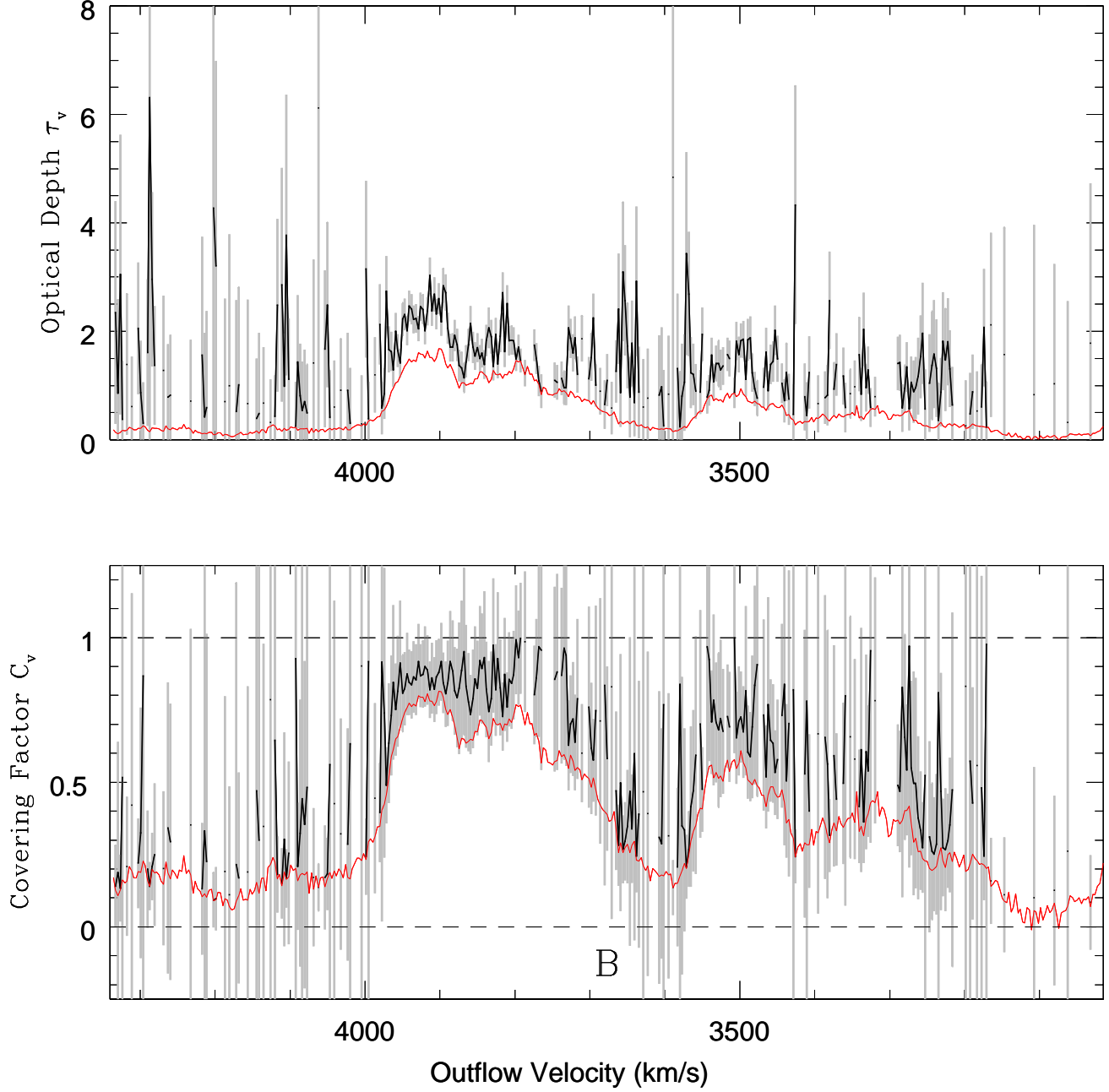


Fig. 4. The thick black line gives the optical depth (top) and covering factor for Ca II as a function of velocity in the (unblended) velocity regime B, after binning by 5 pixels in the dispersion direction. Points are plotted only when a physical solution is possible at that velocity. The grey areas show the ± 1 uncertainty ranges, which can exceed the range of physical solutions (namely, $0 \leq C_v \leq 1$, shown by the dashed lines in the bottom panel). The thin red line in the top panel shows the minimum optical depth needed to match the observed Ca II 3934 absorption in the limit of 100% covering. The thin red line in the bottom panel shows the minimum covering factor needed to match the observed Ca II 3934 absorption in the limit of infinite optical depth. See §4.3.2 for discussion.

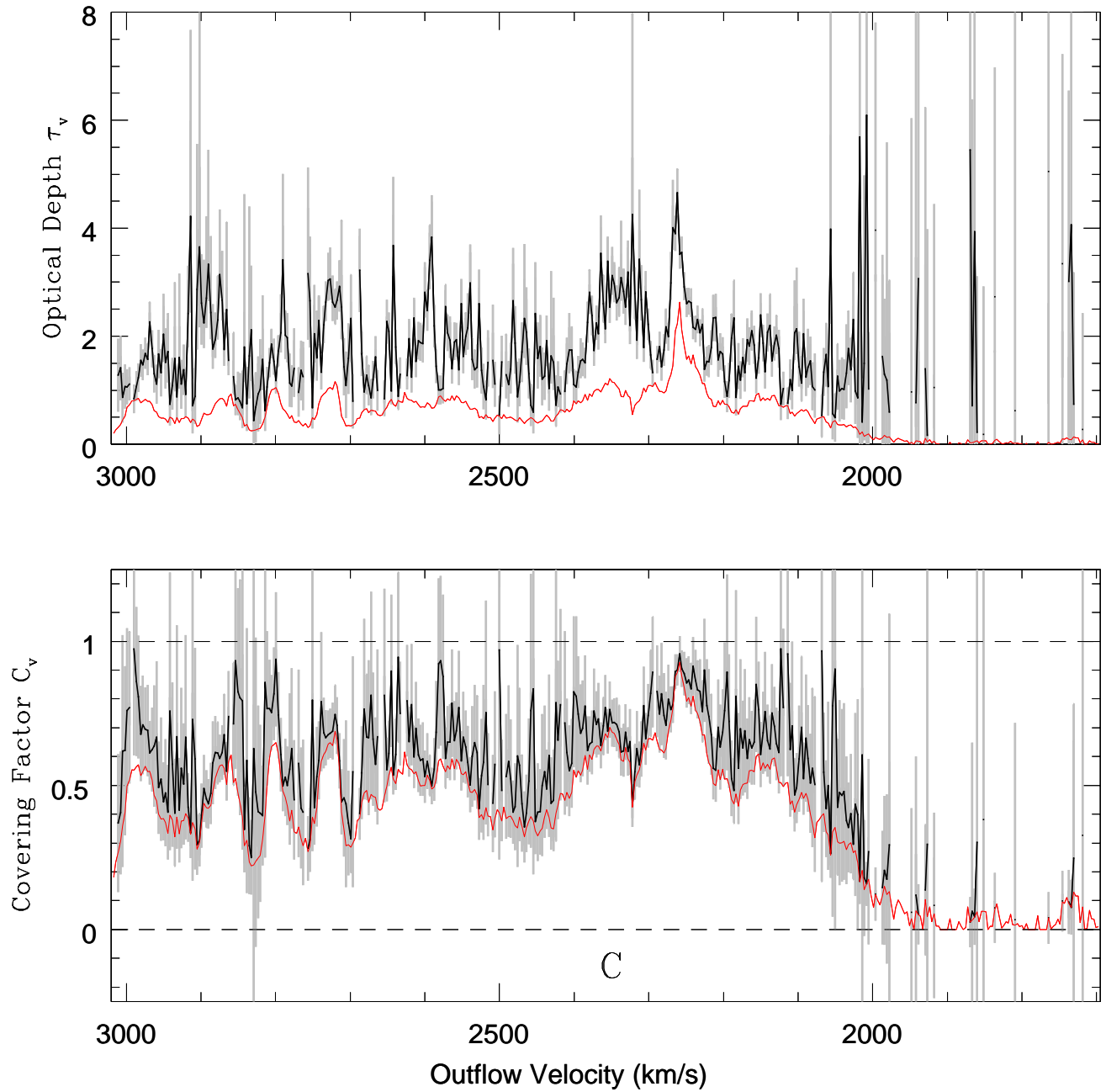


Fig. 5. Optical depth (top) and covering factor for Ca II as a function of velocity in the (blended) velocity regime C, after binning by 5 pixels in the dispersion direction. Symbols as in Figure 4. The uncertainty ranges (grey areas) include the systematic uncertainties from the assumptions made in order to remove the blended absorption, but the random errors almost always dwarf the systematic uncertainties. See §4.3.4 for discussion.

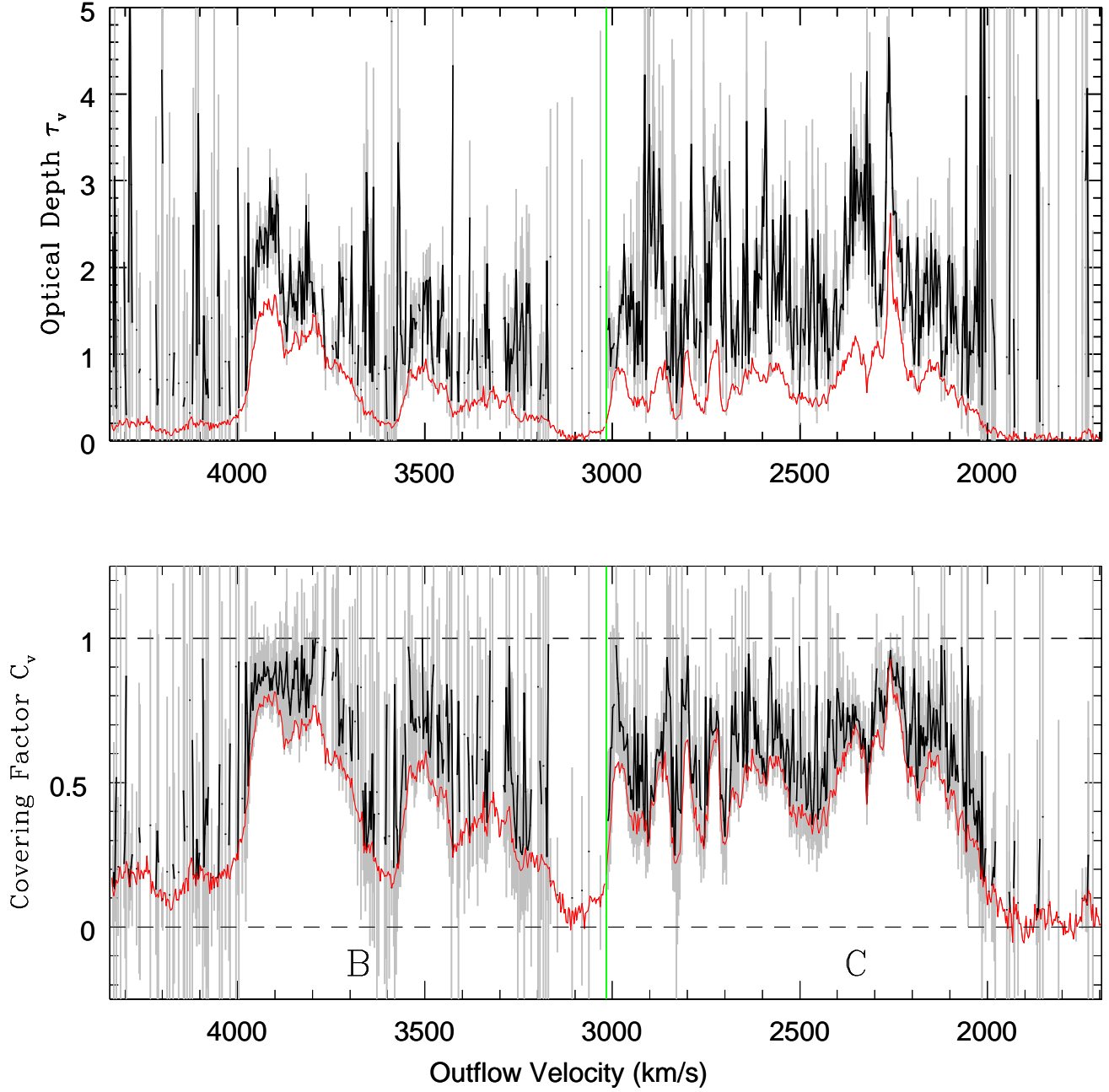


Fig. 6. | Optical depth (top) and covering factor as a function of velocity for the Ca II absorption, after binning by 5 pixels in the dispersion direction. Note that the optical depth scale is different than in the previous two Figures. The green vertical line at 3017 km s^{-1} separates velocity regimes B and C; other symbols as in Figure 4. See §4.3.5 for discussion.

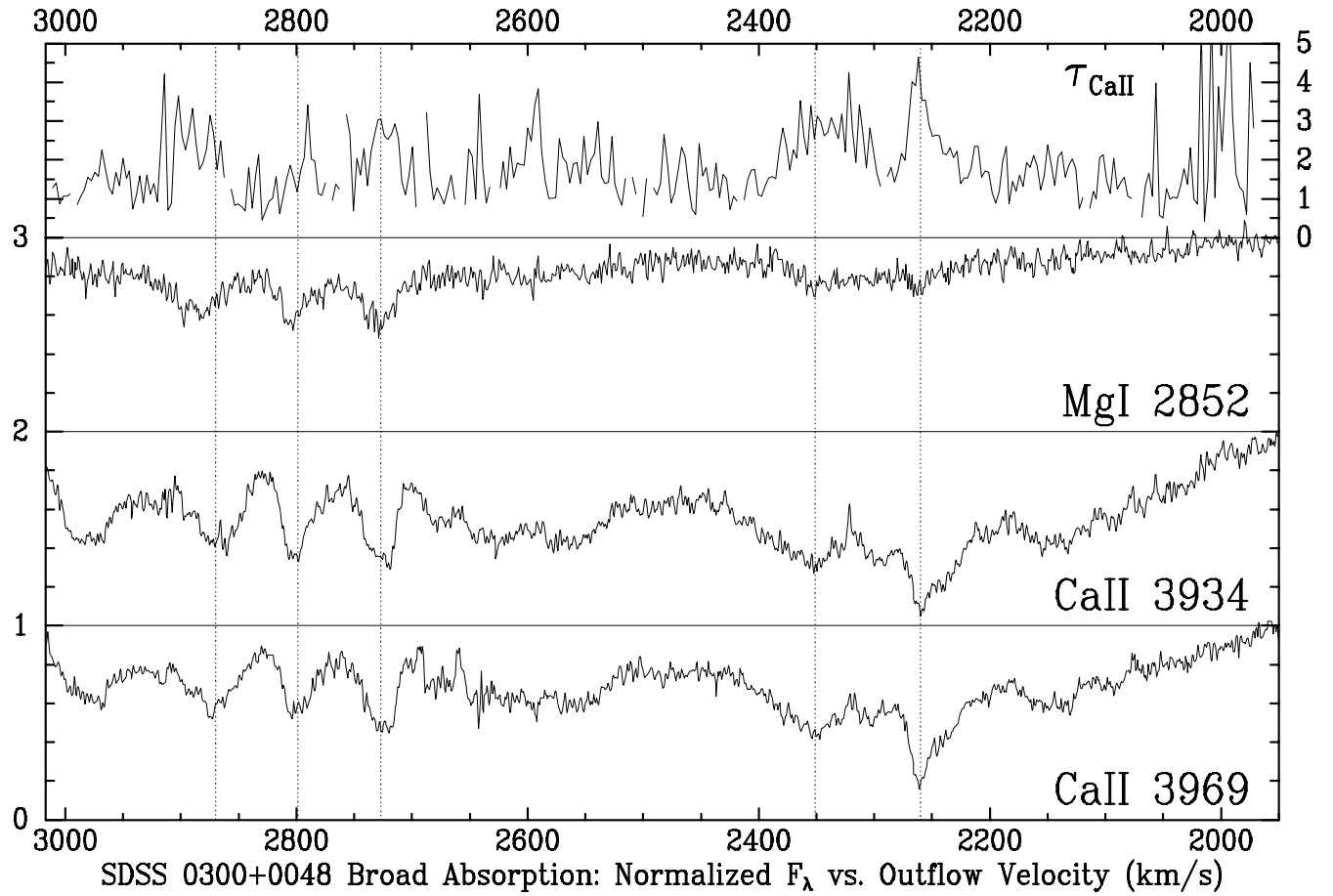


Fig. 7. Close-up of velocities where strong Mg I absorption is present in the BAL outflow. The uppermost panel and right-hand scale show the Ca II 3934 optical depth. The lower three panels show normalized intensities in the Mg I 2852, Ca II 3934, and Ca II 3969 regions, the latter corrected for narrow, blended associated Ca II 3934. The Mg I region normalization is uncertain: it is unclear whether there is Mg I absorption at 2400–2700 km s^{−1} or not. See §4.3.6 for discussion.

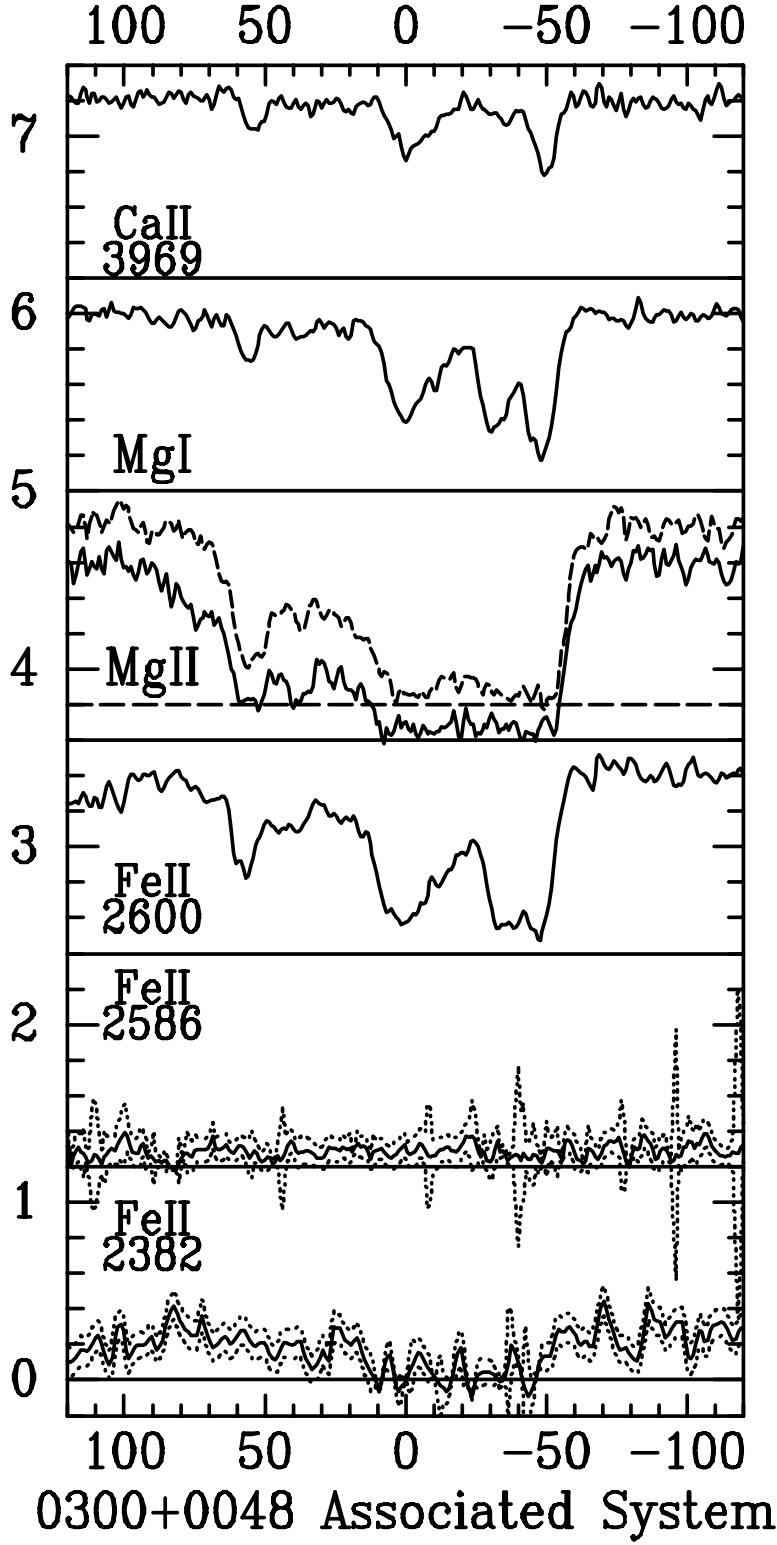


Fig. 8. | Transitions in the associated absorption system in SDSS 0300+0048. The horizontal scale is the velocity in km s^{-1} (positive values for out flow). Each transition shown has been offset from the next by 1.2 normalized flux units in the vertical direction. Both lines of the Mg II doublet are plotted; the 2803 line is plotted as a dotted line offset by +0.2 flux units. For two of the Fe II transitions dotted lines are plotted to show the ± 1 uncertainty ranges.

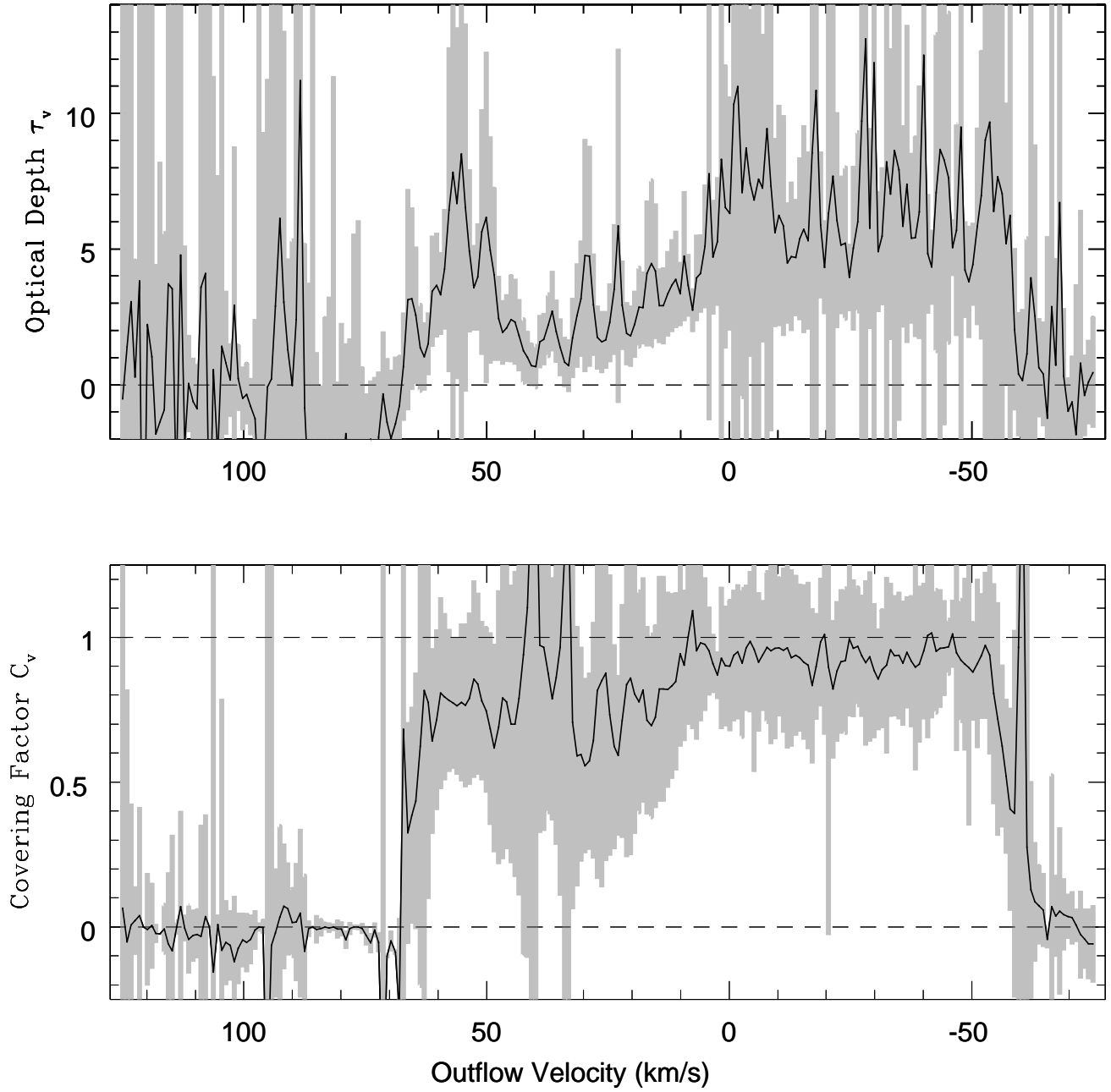


Fig. 9. The thick black line gives the optical depth (top) and covering factor for associated Mg II as a function of velocity. The grey areas show the ± 1 uncertainty ranges. The dashed lines delimit the ranges of physically valid solutions; namely, $\tau_v > 0$ and $0 \leq C_v \leq 1$.

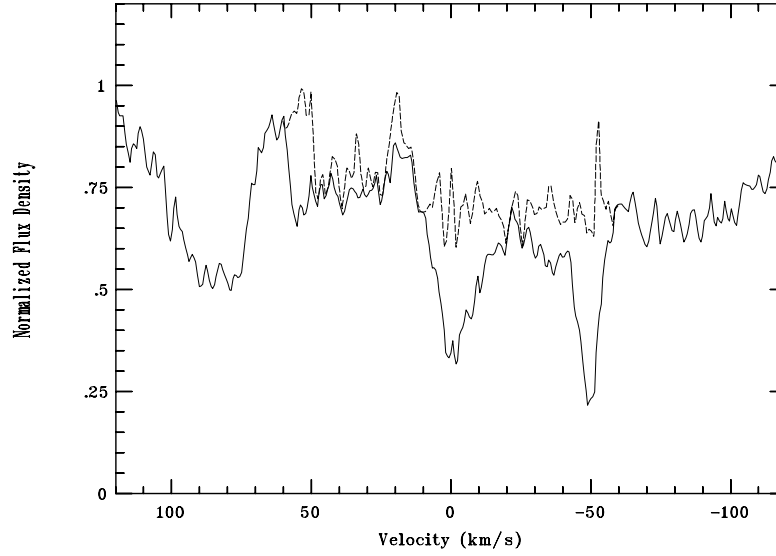


Fig. 10. The region of the Ca II 3969 BAL trough around the wavelength of associated Ca II 3934 absorption. The solid line shows the observed, normalized spectrum, and the dashed line the spectrum with the associated Ca II 3934 removed using the Ca II 3969 profile and estimates for the optical depth and covering factor; see Appendix A. The corrected spectrum appears reasonable everywhere except for a narrow spike near -53 km s^{-1} .

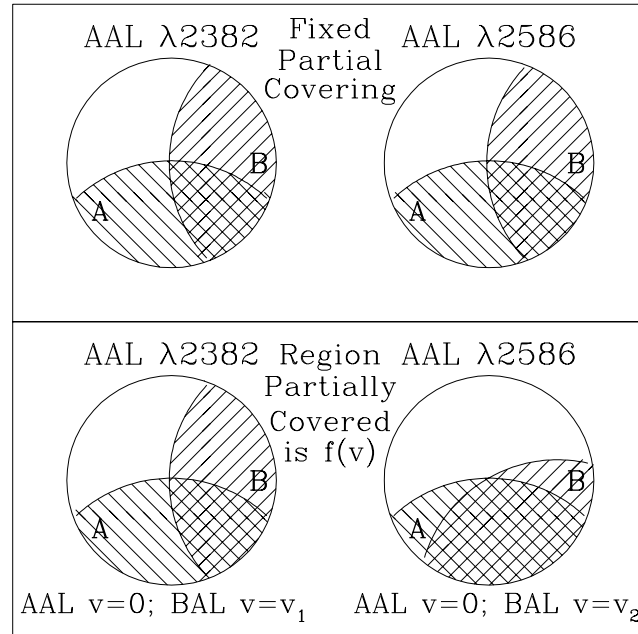


Fig. 11. Schematic model of a quasar (circle) and absorption with partial covering. The lines slanting down and to the right show the source region covered by the narrow, associated, ground-state Fe II absorption (A), while the lines slanting up and to the right show the source region covered by the broad, excited Fe II absorption (B). The partial covering is shown at the redshifted wavelength of the associated Fe II 2382 Å absorption on the left, and at the redshifted wavelength of the associated Fe II 2586 Å absorption on the right. As discussed in the text, the spatially fixed partial covering shown in the top panel cannot explain our observations. Instead, our data indicate that the broad absorption trough covers different regions of the quasar as a function of velocity, as shown in the bottom panel.